JOPSS
JAEA Originated Papers Searching System

日本原子力研究開発機構機関リポジトリ
Japan Atomic Energy Agency Institutional Repository

Title	Year-round variations in the fluvial transport load of particulate ^{137}Cs in a forested catchment affected by the Fukushima Daiichi Nuclear Power Plant accident
Author(s)	Matsunaga Takeshi, Nakanishi Takahiro, Atarashi-Andoh Mariko, Takeuchi Erina, Muto Kotomi, Tsuzuki Katsunori, Nishimura Shusaku, Koarashi Jun, Otosaka Shigeyoshi, Sato Tsutomu, Miyata Yoshiki, Nagao Seiya
Citation	Journal of Radioanalytical and Nuclear Chemistry, 310(2), p.679-693
Text Version	Author's Post-print
URL	https://jopss.jaea.go.jp/search/servlet/search?5054679
DOI	https://doi.org/10.1007/s10967-016-4840-3
Right	This is a post-peer-review, pre-copyedit version of an article published in Journal of Radioanalytical and Nuclear Chemistry. The final authenticated version is available online at: http://dx.doi.org/10.1007/s10967-016-4840-3.

Japan Atomic Energy Agency

Year-round variations in the fluvial transport load of particulate ^{137}Cs in a forested catchment affected by the Fukushima Daiichi Nuclear Power Plant accident

Takeshi Matsunaga[1], Takahiro Nakanishi[1], Mariko Atarashi-Andoh[1], Erina Takeuchi[1], Kotomi Muto[1], Katsunori Tsuduki[1], Syusaku Nishimura[1], Jun Koarashi[1], Shigeyoshi Otosaka[1], Tsutomu Sato[2], Yoshiki Miyata[3], Seiya Nagao[3]

[1]*Nuclear Science and Engineering Center, Japan Atomic Energy Agency, Ibaraki 319-1195, Japan*

[2]*Division of Sustainable Resources Engineering, Graduate School of Engineering, Hokkaido University, Sapporo 060-8628, Japan*

[3]*Low Level Radioactivity Laboratory, Institute of Nature and Environmental Technology, Kanazawa University, Kanazawa, Ishikawa 923-1224, Japan*

Correspondent: Takeshi Matsunaga

Tel.: +81 29 282 6860; Fax: +81 29 282 6760

E-mail address: matsunaga@istc.int

Abstract

Particulate ^{137}Cs was collected from stream water for 2 years to assess the long-term trend of ^{137}Cs discharge from a forest after the Fukushima Nuclear Power Plant accident. A seasonal increase in the fluvial transport load of particulate ^{137}Cs in suspended solids (SS) was observed in July–October when rainfall was abundant. The ^{137}Cs load was controlled by the SS load. This control was attributed to cesium affinity for phyllosilicate clay minerals as verified by the low extractability of particulate ^{137}Cs. These findings indicate the fluvial particulate ^{137}Cs load is significantly related to the climate and geomorphological features of Japan.

Keywords

Fukushima Daiichi Nuclear Power Plant accident, forest, radiocesium, suspended solids, fluvial transport load, seasonal variation

Introduction

A large amount of radionuclides was released into the atmosphere following the Fukushima Daiichi Nuclear Power Plant (NPP) accident [1-3] triggered by the Great East Japan Earthquake (March 11, 2011). Among the various radionuclides released [4, 5], the ^{134}Cs (a half-life of 2.065 y) and ^{137}Cs (a half-life of 30.04 y) isotopes caused long-lasting environmental contamination [6-7].

A major part of the affected area is located in hilly, forested catchments because of the regional geography [8]. Moreover, some forests are located near residential areas and offer economic opportunities. Therefore, the fate of the radioactive fallout in the forest has been a central issue in radioecology following the Fukushima Daiichi NPP accident [*e.g.*, 9].

We previously investigated the vertical migration of ^{137}Cs with water seepage through the forest floor [10], and the redistribution of ^{137}Cs on a forested hill slope via biological processes [11], and the spatial variation in air dose rates due to the radiocesium deposited on the forest floor [12].

In addition to these ^{137}Cs dynamics in the vegetation-soil system, the discharge of ^{137}Cs into streams through forested catchments is important [*e.g.*, 13]. This is typically a unique outflux of the fallout radionuclides from the forest ecosystem and should be considered in the radionuclide balance of the forest ecosystem. In addition, running water from the catchments is used by industries, and for irrigation and drinking water [*e.g.*, 14].

Various studies have been conducted regarding how river systems have been affected by this accident. Sakaguchi et al. [15] provided an early investigation of water body contamination in the Abukuma River Basin near the NPP. The peculiar importance of the particulate form of ^{137}Cs in fluvial transport under high flow conditions was assessed during the first 6 months after the accident [16]. Studies concerning the migration of ^{137}Cs in small catchments during storm events were also performed [17-19]. The solid-phase transport of ^{137}Cs from upstream to midstream was investigated through a bed sediment analysis in the Abukuma River Basin [20, 21]. Research by Sakaguchi et al. [22] enhanced our understanding of this subject by addressing the characteristics of suspended solid (SS) along tributaries and the main stream of the Abukuma River Basin. Yoshimura et al. [23] presented a dataset with partitioning between the particulate and dissolved forms of ^{137}Cs at 30 locations in the Abukuma and other river basins. Tsuji et al. [24] discussed the relationship between the ground deposition density and the occurrence of ^{137}Cs in adjacent rivers.

These studies are all important for understanding the behavior of the ^{137}Cs derived from the Fukushima Daiichi NPP accident in the river system. However, the period of the consecutive field observations of these studies was limited, spanning up to 6 months [16, 18], although a recent report on dissolved ^{137}Cs concentration variations studied a three year period [25]. In addition, the sampling frequencies in these studies were generally limited to once or twice per month.

According to reports of ^{137}Cs derived from weapons testing [*e.g.*, 26-28] and the case of the Chernobyl accident [*e.g.*, 29], the discharge of atmospherically derived radionuclides into rivers from catchments lasts more than several decades. Therefore, it is important to conduct long-term observations to accurately understand and describe the effects of this contaminant over time. Here, we report long-term observations of the fluvial ^{137}Cs transport following the Fukushima Daiichi NPP accident in a pristine river located in a mountain catchment. In our observations, we conducted a continuous and unmanned collection of suspended solids.

The difficulties encountered when conducting long-term observations include the sample collection workload during stochastic rainfall events. We developed a passive, integrated collection system for SS and dissolved components to conduct long-term observations [30]. The technological details of the system, the performance of SS collection over 1.5 y, and the ^{137}Cs results of four collection periods were described in our previous paper [30].

This study involves an additional 6 months of data to the dataset of the previous paper on SS collection [30]. This expansion enables us to do comprehensive discussions on seasonal and annual variations in the fluvial ^{137}Cs flux for the continuous 2 y dataset from December 2011 to December 2013, including ^{137}Cs extractability from SS and SS mineralogy.

Materials and methods

Study site

The study site is a 0.6 km^2 forested catchment located in the northern region of the Abukuma Mountains (Fig. 1) approximately 70 km southwest from the Fukushima Daiichi NPP (N 36° 55′ 30″ (36.925 in decimal degrees)–N 36° 55′ 50″(36.931), E 140° 35′ 00″(140.583)–E 140° 35′ 40″(140.594)). The site was affected by radioactive fallout from the Fukushima Daiichi NPP accident and received 10–60 kBq m^{-2} of ^{137}Cs deposition according to an aerial survey [6].

The study site is hilly with an elevation range of 588–724 m [31]. Several small steep faces and lowlands collectively form a single valley with a stream. This stream is a pristine source for the Shitoki River, which meets the main stream of the Same River 20 km downstream before flowing into the Pacific Ocean.

The annual mean precipitation at the site is 1,910 mm, and the annual mean temperature is 10.7°C [32]. More than half of the annual precipitation occurs from May to October. Seasonal storm events (i.e., typhoon) with heavy rainfall occasionally hit the area during July–October [18]. Seasonally dense precipitation and typhoons are common along the Pacific seaboard of Japan. At the study site, snow is present at a depth of up to 20 cm from the end of January to the beginning of March. The surface soil is brown forest soil and supports a developed deciduous forest. Included in the forest canopy are *Fagus crenata*, *F. japonica, Quercus serrata*, *Kalopanax pictus*, and *Acer mono f. marmoratum* [33]. At the time of the accident, the trees had shed their leaves and the ground was covered with snow.

Sample collection

The SS sampling point was the downstream portion of 90% of the catchment area (Fig. 1). A small-scale filtration system was used during a preliminary sampling period from September to November 2011. It comprised three sequentially connected short (250 mm long), polypropylene-wound cartridge filters with pore sizes of 100 μm, 10 μm and 0.5 μm. After December 2011, a large-scale, passive, integrated collection system that we developed was employed [30]. In this system, a portion of the river water was led to a filtration system on a bank by using the natural decline in the riverbed level. The study site is a shallow stream with a rocky riverbed. The natural configuration of rocks on the riverbed creates relatively deep points where stream water flows even during low-flow periods. The intake was set at one of these points, where water was not stagnant. The intake had an aluminum funnel (7.5 cm in diameter) at the top of a vinyl hose. The section of the funnel was placed in the middle of the stream against the flow. The inlet was covered with a net of approximately 3 mm mesh to stop the entry of large obstacles such as dead leaves.

The filtration system comprised two types of cartridge filters with nominal pore sizes of 100 μm and 0.5 μm. An important feature of the filter material (polypropylene) was that SS were easily detachable by washing the yarn with water after dismantling the filters. The water flow rate through the system was approximately 1.5–2.5 L min^{-1}. The flow rate and the cumulative amount of water that passed through were monitored using an inline flow meter (LW10-TTN, Horiba STEC, Kyoto, Japan). An integration period of 20–40 d was chosen considering the cumulative amount of precipitation during the period. The SS from the river were recovered in the laboratory from the cartridge filters and the bottoms of the filter vessels (muddy deposit). The SS samples were size fractionated into the following four fractions: 2000 μm (2 mm) – approximately 3 mm (termed F1), 500–2000 μm (F2), 75–500 μm (F3), and <75 μm (F4).

To evaluate the collection efficiency of the system for SS, the river water discharged from the system was further passed through four short cartridge filters (250 mm length) with a pore size of 0.5 μm (backup filters), which were set in parallel. This evaluation was conducted during three selected collection periods in late 2013.

Monitoring of hydrological conditions and turbidity

The stream water flow rate was evaluated by monitoring the water depth using a rectangular weir (Fig. 1) originally installed by Abe et al. [31] for a forest ecology study. The water depth at the weir was recorded every 20 min (until 8-May-2013) or every 15 min (after 8-May-2013) using a pressure gauge (SS-202-10M-30, KENEK, Tokyo, Japan). The validity of the weir formula was confirmed by manually measuring the water flow at the weir using an electromagnetic flow meter (VP-1000, KENEK, Tokyo, Japan) and scaling the water depth at the weir. The weir was occasionally cleaned for sand deposition. Precipitation was recorded hourly by rain gauges installed in an open plot adjacent to the catchment. A throughfall gauge set nearby the stream water collection point was used when an open rain gauge developed a technical problem. Turbidity (NTU) was recorded every 15 min with a water quality monitor (U-20XD, Horiba, Kyoto, Japan) set adjacent to the depth monitor.

Laboratory analysis

Radioactivity analysis of suspended solids

The ^{137}Cs concentrations in the size-fractioned SS samples were measured using gamma-ray spectrometry with germanium semiconductor detectors (GEM20P4-70, GEM25P4-70, GEM20, GWL-120230 and LO-AX-51370/20P, ORTEC, Oak Ridge, USA). Certified volumetric sources of multi-nuclides (EG-ML, Eckert & Ziegler Isotope Products, Valencia, CA, USA; MX033U8PP, Japan Radioisotope Association, Tokyo, Japan) were used to calibrate the germanium detectors. A quality control was completed by participation in an intercomparison test organized by International Atomic Energy Agency amnd the Tsukuba University (IAEA-TEL-2011-8), which employed reference materials of soil samples including ^{137}Cs; water, aerosol filters and grass samples including ^{137}Cs and ^{134}Cs. The test showed that our laboratory ranked as the one of the best two laboratories among 19 ones.

Mineralogy of suspended solids

The finer size fractions of the SS (F3 and F4) were analyzed to characterize the ^{137}Cs-bearing materials. Mineralogical analyses were performed for selected sampling runs representing the various seasons throughout the year. A traditional powder X-ray diffraction (XRD) method (random orientation) was used for a bulk material analysis on an X-ray diffractometer (RINT 1200, Rigaku, Tokyo, Japan). The spectrum analysis was based on the Hanawalt method [34], and clay minerals were identified for the oriented samples and prepared as follows (powder orientation) [35]: Approximately 10 mg of ground sample was mixed with 20 μL of water. The sample was dispersed by ultrasonic treatment. An aliquot of the slurry was transferred with a pipette and spread on a glass plate. The glass plate was allowed to stand for more than 24 h until it dried. Next, the samples were subjected to the same instrumental analysis used for the powder diffraction experiments.

Extraction of ^{137}Cs from suspended solids

To estimate the exchangeability of the particulate ^{137}Cs, an extraction experiment was conducted on the F3 and F4 fractions. Extraction with ammonium acetate was used because this method has been frequently reported in the literature [*e.g.,* 36-37], and it has also been applied to the case of the Fukushima NPP accident [38]. This wide use of the same method allows for a meaningful comparison among different studies. One gram of freeze-dried SS sample was mixed with 10 mL of ammonium acetate (CH_3COONH_4, pH 7) in a centrifuge tube and shaken for 2 h at 25°C. Next, the sample was centrifuged at 3,000 rpm (centrifuge model H-103N, Kokusan, Tokyo, Japan), and the supernatant was recovered. The remaining solid was washed by adding an additional 5 mL of purified water and centrifuging. The supernatants from the ammonium acetate and single water-wash treatment were combined as an ammonium acetate-extractable fraction for the radiocesium measurements. The radioactivity of the samples in the centrifuge tubes before extraction accounted for 100% of the radioactivity in the original sample. All radioactivity analyses were conducted by gamma-ray spectrometry at Kanazawa University (KU) with EGPC 90-220-R, EGM 3800-30-R, EGMP 60-30-R detectors (CANBERRA, Meriden, USA).

Evaluation of transport load of suspended solids and ^{137}Cs

The transport load of the SS and that of ^{137}Cs contained in the SS were evaluated for each large-scale filtration sampling period (R9–R26). The SS mass transport load was defined as the weight of SS (kg) transported with the cumulative river water discharged at the study site. For the purpose of comparison, the cumulative SS load was normalized to a mean daily value over the sampling period. The ^{137}Cs load was defined as a product of the SS mass load and the ^{137}Cs concentration in each size fraction. Detailed derivations of the two loads are provided in Appendices 1 and 2.

Results

Suspended solids mass load

Table 1 lists the results of the SS collection at the study site from December 2011 to

December 2013 (an approximately 2 y hydrological period). Although the collection system was inoperative several times because of obstructions at the river water inlet or freezing in midwinter (February), the system operation rate was 88%. The daily base SS mass transport load had a large range of variation (0.8–96.5 kg d^{-1}) with a mean of 13.7 kg d^{-1}. The finest fraction, F4 (<75 μm) accounted for 90–95% of the total SS (Table 1). The mean contributions by different size fractions over 2 y (R9–R26, December 2011–December 2013) were 0.4 ± 0.4% (within a range from 0.1% to 1.4%) (F1), 1.5 ± 3.5% (within a range from 0.4% to 5.8%) (F2), 8 ± 4% (within a range from 4.5% to 19.0%) (F3), and 90 ± 4% (within a range from 76.9% to 94.7%) (F4).

As a general feature, larger values were observed from July to October in both 2012 and 2013. By contrast, a low load was observed from December to February (R9, R10, R17, R18, and R26). This seasonal variation was similar to that of the precipitation. The relationship of the SS mass load with the amount of precipitation is shown in Fig. 2. The SS mass load (the whole amount including all size fractions) was positively correlated ($r=0.70$, $p=0.01$) with the integrated amount of precipitation.

Particularly large loads were evaluated for R12 and R24 (Table 1). These two runs included extreme rainfall events with the total precipitation of 224 mm on June 20, 2012 (Flood 1, Figs. 3a and 3b) and 220 mm on September 15, 2013 (Flood 3), with a maximum intensity of 48.5 and 66.0 mm h^{-1}, respectively. The calculation using turbidity (Appendix 1) suggested that the SS flux during the 12 h around the peaks of the two extreme flood events contributed 43% and 52% of the sum of Runs 9–17 (mainly in 2012) and Runs 18–26 (mainly in 2013), respectively. On the other hand, one large flood event, the flood-2 (Figs. 3a and 3b) caused by a heavy shower of 90 mm in two hours of July-6-2012, was not observed in our sampling because we stopped the collection system for maintenance during a period that included the event, without anticipation.

Cesium-137 concentration associated with suspended solids

Figure 3c shows the ^{137}Cs concentrations included in SS, which were corrected for radioactive decay at the end of each sampling event (Table 1). Measured concentrations of two cesium radioisotopes (^{134}Cs and ^{137}Cs) are numerically given in Tables S1 and S2 of Supplementary Information, respectively. The results of the collection efficiency evaluation indicated that the ^{137}Cs radioactivity that passed through the main SS collection system (uncollected portion) was only 0.6–1.6% of the sum of the main collection system and the backup filters (see Table S4 of Supplementary information), indicating that almost all SS were collected.

The temporal variation in the ^{137}Cs concentration was characterized by a rapid decrease at the beginning of 2012 (~300 d after the nuclear accident), and it was followed by a gradual decrease until the end of 2013 (Fig. 3c). The ^{137}Cs concentration in the finest fraction (F4) occasionally reached 10 Bq g^{-1} in R1–R9. In addition, the ^{137}Cs concentrations remained lower than 5 Bq g^{-1} and decreased to ~3 Bq g^{-1} within 660 days (R10–R26: February 29, 2012–December 17, 2013).

Regarding the dependency of the ^{137}Cs concentration on the size fractions, the finest fraction (F4) possessed the highest ^{137}Cs concentration. In a few cases, the second finest fraction (F3) was comparable with that of F4 based on our earlier observation period (e.g., R1 and R7). Notably, the coarse fraction (F1), which consisted of fine litter fragments, occasionally exhibited a ^{137}Cs concentration equivalent to or greater than that measured in F4 (i.e., R11, R18, and R23).

Mineralogical result of suspended solid constituents

Quartz, plagioclase, and amphibole were components of the primary minerals in the SS (Fig. 4a). The distinct presence of plagioclase and amphibole, which are relatively sensitive to weathering, suggests that the SS contained comparatively "young" materials. More quartz and plagioclase were found in F3 than F4 (Figs. 4a, 4b). The F4 XRD profiles of the selected samples from various seasons are shown in Fig. 4c. The clay minerals vermiculite, mica and kaolinite were also commonly found in the SS. Background XRD signals at ~20° were observed in F4 and slightly in F3 (data not shown). These background signals may correspond to amorphous or organic materials. In the F4 size fraction, plagioclase was relatively outstanding in low water conditions (R16, R17, and R19) compared to a period of abundant rain season (R21 and R24). Except this feature, the mineralogical composition of SS exhibited no appreciable seasonal variations. This mineralogical homogeneity might be relevant to the uniformity of the particle size distribution of SS (Table 1).

Results of ^{137}Cs extraction

The proportions of ^{137}Cs extracted with 1 M ammonium acetate (pH 7.0) for selected samples (i.e., R18, R19, R20, and R21) are shown in Fig. 5a. The extracted proportion was low (range, 0.5–1.7%) except for one case (i.e., 5.1% for the R18 F3 sample). The 5.1% value is still a minor fraction of the entire amount of ^{137}Cs in the tested SS samples. Fig. 5b shows the original ^{137}Cs concentration in the tested SS samples. The extracted proportion was low and independent of the size fraction and original ^{137}Cs concentrations.

Discussion

Considerations on methodology of suspended sediment collection

Correction for SS transport load

The SS transport load is a product of SS concentrations and flow rate. The load dynamically changes with river flow conditions in terms of those two values. Ideally, an amount of SS collected at every instance shall be proportional to the dynamically changing load. This might be realized by increasing a collection rate of river water proportionally to a river water flow rate (a flow-weighted collection method). If this collection method was realized, the integration of the collected SS would be a some down-sized value of an actual SS load during a collection period. However, this type of collection method cannot be realized practically [30].

In the present study, the river water collection rate was kept at an almost constant rate through out the collection period (a time-integrated collection method). The rate was determined by a geographical condition (the drop head from the inlet of the collection hose to the filter vessel), not by dynamic hydrographical conditions.

If a SS load is calculated by using a ratio of the accumulated water passed through the SS collection system to the total river water flux during a collection period, the load would be underestimated. This is because the collection rate in this method was not proportional to an instantaneous, actual river water flow rate. A fraction of collected water mass become relatively smaller during high water flow periods compared to low water periods. The SS concentration generally increases during high water flow periods. Therefore, the aforementioned smallness in the fraction of collected water mass leads to underestimation of the SS load which cannot be simply compensated by the ratio of water mass.

We evaluated the degree of this underestimation by simulating the time-integrated load and the flow-weighted load by using the turbidity record and flow rate record of every 15 minutes. The degree was expressed in a form of correction factors for the load in a time-integrated collection. Here, we considered the turbidity well approximates the SS concentration [39]. Although a complex relationship between the turbidity and the SS concentration has been reported for extreme flooding events [40, 41], the linear assumption has been proven in various Japanese rivers [39, 42, 43]. The equations used in the correction are given in Appendix 1, along with the correction factors for each run (Table A1 in the Appendix).

Representativeness of collected SS samples

The present method is not a flow-weighted SS collection as described above. If the nature of SS is largely different depending on hydrological conditions, the nature of the collected SS could be biased.

A possible alteration in the SS may be lowering of ^{137}Cs concentration under high flow conditions due to the increased inclusion of bank and riverbed materials, which could be less contaminated with the radioactive fallout compared with the top surface soil in a forest. However, a plot of the ^{137}Cs concentration (averaged over different size fractions) versus the daily average precipitation does not indicate a clear trend with the daily averaged precipitation ($p>0.38$) (Fig. 6a) or with the daily averaged water discharge ($p>0.23$) (Fig. 6b), nor the SS mass load ($p>0.32$) (Fig. 6c). This implies a lack of dependence of ^{137}Cs concentration on hydrological conditions at the study site.

Kinouchi and Onda [44] addressed the dependence at a tributary of the Abukuma River, the catchment of which was also affected by the Fukushima NPP accident. They reported that the ^{137}Cs concentrations varied from approximately 5 to 30 (Bq g^{-1}), and the variation was independent of the SS concentration up to 250 mg L^{-1}. Ueda et al. [17] also reported that no systematic variations in ^{137}Cs concentration were observed for SS concentrations in two small streams to the north of the Fukushima Nuclear Power Plant.

These results suggest that the SS samples collected in this study represent the average ^{137}Cs concentration of transported SS over each sampling period as a first approximation.

Temporal variations in the ^{137}Cs concentrations in the SS

As indicated in Result section, the ^{137}Cs concentration decreased rapidly from September 2011 (0.5 y after the accident) until the beginning of 2012, and then decreased gradually until the end of 2013 (Fig. 3c). This rate of decrease was considerably faster than that due to radioactive disintegration (–2.3% y^{-1} for ^{137}Cs), and it diminished with time. The relevant processes that contribute to a decreasing particulate ^{137}Cs concentration over time may include (a) vertical migration into deeper soil strata, (b) physicochemical fixation to soil constituents over time, and (c) changes in soil erosion processes due to heavy rainfall events. Nakanishi et al. [10] reported that the vertical migration of ^{137}Cs into deeper soil layers was limited in our catchment. In a different forested plot, we found a strong fixation of ^{137}Cs to surface soil within the first 3 months after the Fukushima Daiichi NPP accident [45]. These results suggest that ^{137}Cs remained in surface litter and surface soil and that fixation to soil had already been established before September 2011. Therefore, the former two processes could not sufficiently explain the temporal changes in the ^{137}Cs concentration in the SS. The last hypothesis (c) is probable because heavy precipitation related to typhoons or along active fronts likely redistributes easily erodible, polluted soil surfaces in ephemeral streams. In particular, Typhoon Roke in September 2011 discharged significant quantities of radiocesium into rivers in Fukushima Prefecture [16, 18]. This may have contributed to the rapid decrease in the ^{137}Cs concentration in the stream SS until the beginning of 2012.

Fluvial transport load of particulate ^{137}Cs

The particulate ^{137}Cs load is illustrated in Fig. 7. Numerically, in Table S5 of Supplementary information. One remarkable feature is that the seasonal variation in the ^{137}Cs load is reproducible over the 2 y period (2012 and 2013). The particulate load exhibited a characteristic seasonal change: it was low during the collection periods from November to March (R9–R11, R18–R20, and R26), while higher values were observed from July to October (R13–R16, and R22–R25).

A comparison of Fig. 7 with the SS mass load (the column mass load, Table 1) indicates that the ^{137}Cs load that was nearly exclusively controlled by the SS mass load. The variation in the ^{137}Cs load was tightly correlated with the rainfall events, which typically increased the SS mass load. This macroscopic feature is considered to have a link to microscopic characteristics. The present extraction experiment indicated a low proportion of ^{137}Cs extracted by 1 M ammonium acetate in the fine SS fractions (Fig. 5). The mineralogical analysis revealed that several types of silicate clay minerals were always present in the SS (Fig. 4c). These phyllosilicate clay minerals strongly adsorb Cs ions [34, 46]. Accordingly, most of the ^{137}Cs was strongly associated with the fine SS fractions.

The finest fraction (F4) surpassed the other fractions in terms of SS (Table 1, Fig. 2). The mean contribution of F4 to the particle size distribution was 90%, with a standard deviation of 4% (Table 1). This result is consistent with the suggestion by Tanaka et al. [21], who studied the midstream area of the Abukuma River. These authors suggested that particulate ^{137}Cs was selectively transported from upstream by fine particles. The present results from a pristine stream further imply that size selection had already occurred, at least in part, during the transport of the eroded surface soil particles from the ground to the stream, as suggested by He and Walling [47].

The particulate ^{137}Cs load had a distinctly large value in R12 and R24 (Fig. 7). This extent corresponds to the large SS load related to extreme rainfall events (Fig. 3b). In our collection, one large flood event (flood-2, Fig. 3b) was not included. Therefore, the real annual load of 2012 must be larger than the present calculation, presumably by 1.5–2-fold (see the description in the Results section for suspended solid mass load related to Fig. 3b).

Consideration of possible inter-annual variation in particulate ^{137}Cs loads

Inter-annual variations in precipitation would cause a yearly difference in the SS mass load. Abe et al. [31] reported a multi-year record of monthly precipitation at the study site during 2001–2006. In their record, the inter-annual variations reached 1.5 times the annual precipitation, with a mean of 1,832 mm (range, 1,604–2,328 mm). In this study, the annual precipitation of 2,139 mm in 2012 decreased to 1,697 mm in the following year (2013). Such inter-annual variations could be expected to occur repeatedly hereafter. Accordingly, the SS mass load could be largely influenced by the inter-annual variation in precipitation. In addition, if an extreme rainfall event occurs, the single event could significantly contribute to the annual load, e.g., more than half of the total.

Implications of this study

Significance of long-term observation

In the present study, the meaning of low- and high-flow periods in terms of the annual particulate ^{137}Cs load was evaluated. This quantitative analysis would not have been possible without actual observations spanning one hydrological year. Furthermore, our 2 y observation period confirmed a seasonal reproducibility of increases/decreases in the particulate ^{137}Cs load. One year of observation cannot verify the reproducibility of the variation.

Significance of the local hydrology and geomorphology

The Chernobyl accident of 1986 caused radioactive contamination of the surface water bodies of rivers and reservoirs [*e.g.*, 48]. Radionuclide concentrations along with the flow rate were monitored in the Pripyat River system in the vicinity the Chernobyl NPP by frequent manual sampling (2−8 times per month) [49]. This monitoring continued for more than 15 years.

In contrast with Japanese rivers [16-18, this study], the fluvial ^{137}Cs transport load did not exhibit a sensitive increasing response to the flooding events caused by snow melts in spring or by several large precipitation events [*e.g.*, 48]. This contrast must be due to the difference in the geomorphology. The Pripyat River catchment consists primarily of flat ground developed in low land. Therefore, water (precipitation on the ground or river water inundating a plain along the river) does not flow with sufficient force to cause surface soil erosion. Instead, it promotes the dissolution of radionuclides with high solubility (*e.g.*, ^{90}Sr) in the natural environment [29, 48, 50]. Thus, the high sensitivity of the particulate ^{137}Cs load to rainfall events in the present study environment is related to the local hydrology and geomorphology in Japan.

Conclusions

This long-term study revealed a clear seasonal change in the fluvial load of ^{137}Cs associated with SS. This seasonal change was reproducible in 2012 and 2013. A closer examination of this change suggests that the fluvial load of particulate ^{137}Cs was tightly connected to the input load of eroded surface soil as a major source of SS to the stream during rainfall events. This relationship occurs because of the strong adsorption of ^{137}Cs to the SS constituents at the site, which comprises layered clay minerals of kaolinite, vermiculite, and weathered mica, and also due to the comparatively uniform ^{137}Cs concentration in SS as a function of sampling periods.

These hydrological and radiochemical causes are considered to determine the fluvial load of the particulate ^{137}Cs in the forested, hilly catchment affected by the Fukushima Daiichi NPP accident. The particulate ^{137}Cs load was subject to inter-annual variations in rainfall and decreased gradually over a long period of time due to a decrease in the ^{137}Cs concentration in SS. The present findings and discussions in this study indicate that the particulate ^{137}Cs load was sensitive to the inter-annual variations in rainfall, which is related to the local hydrology and geomorphology in Japan.

A progressive decrease in the ^{137}Cs concentration in SS over 2 y indicates that the forest environment remains dynamic in terms of its ability to redistribute radioactive fallout. Such long-term seasonal and temporal variations should be considered in the fate of ^{137}Cs fallout in mountainous regions.

Acknowledgments

The authors express their sincere thanks to Masahiro Hirasawa, Makiko Ishihara, and Kazumi Matsumura for their assistance with extensive laboratory work. The permission to use the preserved forest from the forestry management authorities in Ibaraki Prefecture and the Forestry Agency of Japan is gratefully acknowledged. The use of the weir was kindly permitted by the Forestry and Forest Products Research

Institute. We are also grateful to a landowner for their permission to use an open plot for a precipitation gauge. Aya Sakaguchi inspired T.M. to interpret regional features of the Japanese environmental conditions.

Appendix 1. Equations for the mass transport load of suspended solids

In the reality in the field condition, a continuous monitoring of SS concentration is not possible. In this study, the ratio was estimated using a value for turbidity as, a surrogate for the SS concentration with an assumption of a linear relation between the turbidity and SS concentration.

The SS load was evaluated in the following manner for each sampling period. In the following, the notation i (1, 2, 3, or 4) denotes the size fraction of F1, F2, F3 or F4. First, a nominal SS load from a time-integral collection was evaluated (Step 1). Next, a correction factor for the underestimation associated with the time-integrated method was elucidated using the turbidity record (Step 2). Finally, the probable load expected from flow-weighted collection was evaluated (Step 3). Values of the correction factor are listed in Table A1.

Irregular turbidity records such as very high values under normal flow conditions were replaced with calculated values by a relationship between the flow rate and the turbidity (Fig. A1): $T = 1941\ Q - 25$, where T is the turbidity, Q is the flow rate ($m^3\ s^{-1}$), and $r = 0.60$. For instances of extremely low flow rates, this calculation yields negative values because the regression line has a negative y-intercept. Because a negative turbidity value is not logical, these negative values were artificially converted to 1 (turbidity) as the minimum probable value. The influence of this adjustment is limited because this occurred only at a low flow rate. When the calculation produced a T value larger than 990, which is the upper limit of the used turbidity sensor, T was artificially converted to 990 because the regression line is valid within the dynamic range of the sensor.

(1) Step 1

$$W = w_1 + w_2 + w_3 + w_4 \qquad \text{(A1)}$$

$$f_i = (w_i / W) \times 100 \qquad \text{(A2)}$$

$$ml_{SS,\,i} = W \times 0.001 \times (Q / q) \times f_i \times 0.01 / D \qquad \text{(A3)}$$

$$NML_{SS} = ml_{SS,\,1} + ml_{SS,\,2} + ml_{SS,\,3} + ml_{SS,\,4} \qquad \text{(A4)}$$

where

W	total weight of collected SS in the period	(g)
w_i	weight of collected SS of size fraction i in the period	(g)
f_i	fractional percent of w_i by size fraction	(%)
$ml_{SS,\,i}$	mass transport load of SS for size i	(kg d^{-1})
q	cumulative volume of water passing through the filtration system in the period	(m^3)
Q	cumulative river water discharge over the period	(m^3)
D	duration of the period	(d)
NML_{SS}	nominal total mass transport load of SS	(kg d^{-1})

(2) Step 2

$$CF = \sum_1^N Q_i T_i \;/\; \sum_1^N Q_i \sum_1^N T_i \qquad \text{(A5)}$$

where,

CF	correction factor	(–)
Q_i	stream water flow rate at time i	($m^3\ s^{-1}$)
T_i	turbidity at time i	(NTU)
i	recording time of water flow and turbidity at every 15 min, i = 1, N	
N	the end point of the recording of the run	

(2) Step 3

$$ML_{SS} = NML_{SS} / CF \qquad \text{(A6)}$$

where

ML_{SS}	total mass transport load of SS expected in flow-weighted collection	($kg\ d^{-1}$)

Appendix 2. Equations for radioactivity transport load of ^{137}Cs

Similarly, the radioactivity transport load was evaluated based on the following calculation. In the present context, the radioactivity refers to that of ^{137}Cs.

$$a_i = c_i\, w_i \qquad \text{(A5)}$$

$$A = a_1 + a_2 + a_3 + a_4 \qquad \text{(A6)}$$

$$af_i = (a_i / A)\ 100 \qquad \text{(A7)}$$

$$al_{SS,\,i} = A \times (Q / q) \times af_i \times 0.01 / D \qquad \text{(A8)}$$

$$AL_{SS} = al_{SS,\,1} + al_{SS,\,2} + al_{SS,\,3} + al_{SS,\,4} \qquad \text{(A9)}$$

where

a_i	amount of radioactivity in SS of size fraction i	(Bq)
c_i	radioactivity concentration in SS of size fraction i	(Bq g^{-1})
A	total amount of radioactivity in SS	(Bq)
af_i	fractional percent of a_i by size fraction	(%)
$al_{SS,\,i}$	radioactivity transport load with SS for size i	(Bq d^{-1})
AL_{SS}	total radioactivity transport load with SS	(Bq d^{-1})

Appendix 3. Comparison of radioactivity concentrations of ^{137}Cs and ^{134}Cs

When the two radiocesium concentrations isotopes were decay corrected to the date of the Great East Japan Earthquake (March 11, 2011, a day close to the nuclear accident) (see Table S3 of Supplementary information for used decay correction factors), the ^{134}Cs to ^{137}Cs ratios were all approximately 1.0 (Supplementary Information, Fig. S1). This value matches the reported value of 0.91 as of June 11, 2011, found in a large-scale soil sampling study [7]. Thus, the isotopic composition confirmed that the ^{137}Cs measured in this study originated from the Fukushima Daiichi NPP accident.

References

[1] Katata G, Ota M, Terada H, Chino M, Nagai H (2012) Atmospheric discharge and dispersion of radionuclides during the Fukushima Daiichi Nuclear Power Plant accident. Part 1: Source term estimation and local-scale atmospheric dispersion in early phase of the accident. J. Environ Radioact.109:103–113

[2] Terada H, Katata G, Chino M, Nagai H (2012) Atmospheric discharge and dispersion of radionuclides during the Fukushima Daiichi Nuclear Power Plant accident. Part II: verification of the source term and analysis of regional-scale atmospheric dispersion. J Environ Radioact. 112:141–154

[3] Kobayashi T, Nagai H, Chino M, Kawamura H (2013) Source term estimation of atmospheric release due to the Fukushima Daiichi Nuclear Power Plant accident by atmospheric and oceanic dispersion simulations. J Nucl Sci Technol. 50:255–264

[4] United Nations (2014) In: United Nations Scientific Committee on the Effects of Atomic Radiation (ed), Sources, effects and risks of ionizing radiation, UNSCEAR 2013 Report, Report to General Assembly with Scientific Annexes, Annex A: Levels and effects of radiation exposure due to the nuclear accident after the 2011 great east-Japan earthquake and tsunami, United Nations, New York, pp.110–119

[5] Yamamoto M (2015) Overview of the Fukushima Dai-ichi Nuclear Power Plant (FDNPP) accident, with amounts and isotopic compositions of the released radionuclides. J Radioanal Nucl Chem. 303:1227–1231

[6] MEXT (Ministry of Education, Culture, Sports, Science, and Technology, Japan), (2011) Database and maps on results of the research on distribution of radioactive substances discharged by the accident at TEPCO's Fukushima Daiichi NPP, first upload on 18-10-2011, last updated on 13-10-2014 at the time of access. http://ramap.jaea.go.jp/map/. Accessed on 7 Dec 2014. (in Japanese)

[7] Saito K, Tanihata I, Fujiwara M, Saito T, Shimoura S, Otsuka T, Onda Y, Hoshi M, Ikeuchi Y, Takahashi F, Kinouchi N, Saegusa J, Seki A, Takemiya H, Shibata T (2015) Detailed deposition density maps constructed by large-scale soil sampling for gamma-ray emitting radioactive nuclides from the Fukushima Daiichi Nuclear Power Plant accident. J Environ Radioact. 139:308–319

[8] GSI (Geospatial Information Authority of Japan), 2013. The national atlas of Japan. http://portal.cyberjapan.jp/site/mapuse4/index.html#zoom=4&lat=35.99989&lon=138.75&layers=BTTT. Accessed on 4 Jan 2015. (in Japanese)

[9] FFPRI (Forestry and Forest Products Research Institute), 2014. *Shin-rin to Houshanou* (Potal site for Forests and radionuclides). http://www.ffpri.affrc.go.jp/rad/index.html. Accessed on 2 Jan 2015. (in Japanese)

[10] Nakanishi T, Matsunaga T, Koarashi J, Atarashi-Andoh M (2014) ^{137}Cs vertical migration in a deciduous forest soil following the Fukushima Daiichi Nuclear Power Plant accident. J Environ Radioact. 128:9–14

[11] Koarashi J, Atarashi-Andoh M, Takeuchi E, Nishimura S (2014) Topographic heterogeneity effect on the accumulation of Fukushima-derived radiocesium on forest floor driven by biologically mediated processes. Sci Rep. doi:10.1038/srep06853.

[12] Atarashi-Andoh M, Koarashi J, Takeuchi E, Tsuduki K, Nishimura S, Matsunaga T (2015) Catchment-scale distribution of radiocesium air dose rate in a mountainous deciduous forest and its relation to topography. J Environ Radioact. 147:1–7.

[13] Ministry of the Environment (2015) *Heisei 23 nendo Kohkyo-yoh-sui-iki Houshasei Busshitsu Monitoring Chousa Kekka (Matome)* (FY2011 summary result of radiological monitoring on water bodies for public use). http://www.env.go.jp/jishin/monitoring/results_r-pw-h23.html. Accessed on 2 Jan 2015. (in Japanese)

[14] Fukushima Prefecture (2012) *Nikyu Kasen Sama Gawa Suikei Kasen Seibi Kihon Houshin* (The basic policy to utilize the Same-gawa river system). http://www.pref.fukushima.lg.jp/uploaded/attachment/10215.pdf. Accessed on 28 Dec 2014. (in Japanese)

[15] Sakaguchi A, Kadokura A, Steier P, Tanaka K, Takahashi Y, Chiga H, Matsushima

A, Nakashima S, Onda Y (2012) Isotopic determination of U, Pu and Cs in environmental waters following the Fukushima Daiichi Nuclear Power Plant accident. Geochem J. 46:355–360

[16] Nagao S, Kanamori M, Ochiai S, Inoue M, Yamamoto M (2015) Migration behavior of ^{134}Cs and ^{137}Cs in the Niida River water in Fukushima Prefecture, Japan during 2011–2012. J Radioanal Nucl Chem. 303:1617–1621

[17] Ueda S, Hasegawa H, Kakiuchi H, Akata N, Ohtsuka Y, Hisamatsu S (2013) Fluvial discharges of radiocesium from watersheds contaminated by the Fukushima Daiichi Nuclear Power Plant accident, Japan. J Environ Radioact. 118:96–104.

[18] Nagao S, Kanamori M, Ochiai S, Tomihara S, Fukushi K, Yamamoto M (2013) Export of ^{134}Cs and ^{137}Cs in the Fukushima river systems at heavy rains by Typhoon Roke in September 2011. Biogeosci. 10:6215–6223

[19] Shinomiya Y, Tamai K, Kobayashi M, Ohnuki Y, Shimizu T, Iida S, Nobuhiro T, Sawano S, Tsuboyama Y, Hiruta T (2014) Radioactive cesium discharge in stream water from a small watershed in forested headwaters during a typhoon flood event. Soil Sci Plant Nutr. 60:765–771

[20] Tanaka K, Iwatani H, Sakaguchi A, Takahshi Y, Onda Y (2014) Relationship between particle size and radiocesium in fluvial suspended sediment related to the Fukushima Daiichi Nuclear Power Plant accident. J Radioanal Nucl Chem. 301:607–613

[21] Tanaka K, Iwatani H, Sakaguchi A, Qiaohui, F., Takahashi Y., 2015. Size-dependent distribution of radiocesium in riverbed sediments and its relevance to the migration of radiocesium in river systems after the Fukushima Daiichi Nuclear Power Plant accident. J. Environ. Radioact. 139, 390–397.

[22] Sakaguchi A, Tanaka K, Iwatani H, Chiga H, Fan Q, Onda Y, Takahashi Y (2015) Size distribution studies of ^{137}Cs in river water in the Abukuma Riverine system following the Fukushima Daiichi Nuclear Power Plant accident. J Environ Radioact. 139:379–389

[23] Yoshimura K, Onda Y, Sakaguchi A, Yamamoto M, Matsuura Y (2015) An extensive study of the concentrations of particulate/dissolved radiocaesium derived from the Fukushima Daiichi Nuclear Power Plant accident in various river systems and their relationship with catchment inventory. J Environ Radioact. 139:370–378

[24] Tsuji H, Yasutaka T, Kawabe Y, Onishi T, Komai T (2014) Distribution of dissolved and particulate radiocesium concentrations along rivers and the relations between radiocesium concentration and deposition after the nuclear power plant accident in Fukushima. Water Res. 60:15–27

[25] Ochiai S, Ueda S, Hasegawa H, Kakiuchi H, Akata N, Ohtsuka Y, Hisamatsu S (2015) Spatial and temporal changes of ^{137}Cs concentrations derived from nuclear power plant accident in river waters in eastern Fukushima, Japan during 2012–2014. J Radioanal Nucl Chem:First online: 09 September 2015.

[26] Matsunaga T, Amano H, Yanase N (1991) Discharge of dissolved and suspended ^{137}Cs in the Kuji River, Japan. Appl Geochem. 6:159–167

[27] Matsunaga T, Ueno T, Chandradjith RLR, Amano H, Okumura M, Hashitani H, (1999) A study on ^{137}Cs and mercury contamination in lake sediments. Chemosphere. 39:269–283

[28] Matsunaga T (2000) The fate of several radionuclides derived from atmospheric fallout in a river watershed, In: Markert B, Friese K (eds) Trace elements: their distribution and effects in the environment. Elsevier, Amsterdam, pp.549–564

[29] Freed R, Smith, L, Bugai D (2004) The effective source area of ^{90}Sr for a stream near Chernobyl, Ukraine. J Contam Hydrol. 71:1–26

[30] Matsunaga T, Nakanishi T, Atarashi-Andoh M, Takeuchi E, Tsuduki K, Nishimura S, Koarashi J, Otosaka S, Sato T, Nagao S (2014) A passive collection system for whole size fractions in river suspended solids. J Radioanal Nucl Chem. 303:1291–1295

[31] Abe T, Fujieda M, Kabeya N, Kubota T, Noguchi H, Shimizu A, Tsuboyama Y, Noguchi S（2011）Report of hydrological observations at the Ogawa Forest Reserve (August 2000 to September 2007). Bulletin of FFPRI. 10:291–317 (in Japanese with English Abstract)

[32] Mizoguchi Y, Morisawa T, Ohtani Y (2002) Climate in Ogawa Forest Reserve, In: Nakashizuka T, Matsumoto Y (eds), Diversity and Interaction in a Temperate Forest Community: Ogawa Forest Reserve of Japan. Ecological Studies. 158:

Springer-Verlag, Tokyo, pp.11–18.

[33] FFPRI (Forestry and Forest Products Research Institute) (2003) Forest Dynamics Database. http://fddb.ffpri-108.affrc.go.jp/. Accessed on 28 Dec 2014. (in Japanese)

[34] Moore DM, Reynolds Jr RC (1989) X-ray diffraction and the Identification and analysis of clay minerals. Oxford Univ Press, New York, pp. 202–271

[35] Juge S (1962) Studies on clay minerals in oil-bearing Neogene Tertiary sedimentary rocks of Northwest Honshu, Japan, with a proposal of criteria for analysis of clay minerals in sedimentary rocks. J Japanese Association of Petroleum Technologists. 27:17–54 (in Japanese with English abstract)

[36] Andersson KG, Roed J (1994) The behavior of Chernobyl ^{137}Cs, ^{134}Cs and ^{106}Ru in undisturbed soil: Implications for external radiation. J Environ Radioact. 22:183–196

[37] Rigol A, Roig M, Vidal M, Rauret G (1999) Sequential extractions for the study of radiocesium and radiostrontium dynamics in mineral and organic soils from Western Europe and Chernobyl areas. Environ Sci Technol. 33:887–895

[38] Hirose M, Kikawada Y, Tsukamoto A, Oi T, Honda T, Hirose K, Takahashi H (2015) Chemical forms of radioactive Cs in soils originated from Fukushima Dai-ichi nuclear power plant accident studied by extraction experiments. J Radioanal Nucl. Chem. 303:1357–1359

[39] NILIM (National Institute for Land and Infrastructure Management) (2015) Relation between suspended solids and turbidity in river water. http://www.nilim.go.jp/lab/bcg/siryou/tnn/tnn0594pdf/ks059410.pdf. Accessed on 15 Aug 2015. (in Japanese)

[40] Gomi T, Dan Moore R, Hassan MA (2005) Suspended sediment dynamics in small forest streams of the Pacific Northwest. J Am Water Resource As. 41:877–898

[41] Mizugaki S, Abe T, Maruyama M (2011) Estimation of high level suspended solids concentration during flood events by means of a turbidity meter. http://thesis.ceri.go.jp/db/giken/h23giken/JiyuRonbun/KK-34.pdf. Accessed on 1 Dec 2015. (in Japanese)

[42] Hanashiro K, Omija T, Higa E, Mitsumoto H, Futenma T, Furugen K, Shimoji Y, Tashiro Y (1994) Study on muddy water resulting from soil run off. Bulletin of Okinawa Prefectural Institute of Health and Environment. 28:67–71 (in Japanese)

[43] HAMC (Hokkaido Agricultural M Center) (2015) Relationships between turbidity and suspended solids concentration in stream water for irrigation. http://www.hamc.or.jp/TOPTEST/02_kangaiyousui.pdf. Accessed on 1 Dec 2015. (in Japanese)

[44] Kinouchi G, Onda Y (2013) Understanding of practical situation of migration of radioactive cesium to rivers and its mathematical analysis using a

distributed-parameters model. In: Report to Nuclear Regulatory Authority Council, "Establishment of methodology to grasp long-term effects caused by radioactive materials due to the Tokyo Electric Power Co. Fukushima Daiichi Nuclear Power Plant accident - Fiscal year 25- ", Japan Atomic Energy Agency, Tokyo, Japan. http://fukushima.jaea.go.jp/initiatives/cat03/entry06.html; http://fukushima.jaea.go.jp/initiatives/cat03/pdf06/2-7.pdf. Accessed on 14 Aug 2015. (in Japanese)

[45] Matsunaga T, Koarashi J, Atarashi-Andoh M, Nagao S, Sato T, Nagai H (2013) Comparison of the vertical distributions of Fukushima nuclear accident radiocesium in soil before and after the first rainy season, with physicochemical and mineralogical interpretations. Sci Total Environ. 447: 301–314

[46] Wauters J, Sweeck L, Valcke E, Elsen A, Cremers A (1994) Availability of radiocaesium in soils. Sci Total Environ. 157:239–248

[47] He Q, Walling DE (1996) Interpreting particle size effects in the adsorption of ^{137}Cs and unsupported ^{210}Pb by mineral soils and sediments. J Environ Radioact. 30:117–137

[48] Sansone U, Belli M, Voitsekovitch OV, Kanivets VV (1996) ^{137}Cs and ^{90}Sr in water and suspended particulate matter of the Dnieper River-Reservoirs System (Ukraine). Sci Total Environ.186:257-271

[49] Ueno T, Matsunaga T, Amano H, Tkachenko Y, Kovalyov A, Sukhoruchkin A, Derevets V (2002) Environmental monitoring data around the Chernobyl Nuclear

Power Plant used in the cooperative research project between JAERI and CHESCIR (Ukraine) (Cooperative research), JAERI-Data/Code 2002-024, Japan Atomic Energy Research Institute (present: Japan Atomic Energy Agency), Tokai-mura, Japan, pp.355–388.

[50] Matsunaga T, Ueno T, Amano H, Tkatchenko Y, Kovalyov A, Watanabe M, Onuma, Y (1998) Characteristics of Chernobyl-derived radionuclides in particulate form in surface waters in the exclusion zone around the Chernobyl Nuclear Power Plant. J Contam Hydrol. 35:101–113

Figure titles and captions

Fig. 1 Location of the study site.

Left panel (a), Study location. Middle panel (b), enlarged local area. N, Fukushima Daiichi Nuclear Power Plant (NPP); S, study site. Right panel (c), enlarged study area. H, intake point of river water by hose; W, weir; F, filtration system of river suspended system; R1, open plot rain gauge; R2, rain gauge for throughfall. Numbers of 500, 600, and 700 indicate contours in m (A.S.L.)

Fig. 2 Relationship between the suspended solids load and precipitation.

Plot of the suspended solids per day of the size fraction in the sampling periods. Data are taken from Table 1. Legend: Whole, suspended solids including all size fractions; F1, 2000 μm (2 mm) – approx. 3 mm; F2, 500–2000 μm; F3, 75–500 μm; F4, <75 μm

Fig. 3 Hydrological records and ^{137}Cs concentration associated with suspended solids for the entire sampling periods.

Subplot (a): hourly precipitation record for the entire collection periods; (b): river water discharge; (c): ^{137}Cs concentration associated with suspended solids. Legend for subplot (c): F1, 2000 μm (2 mm) – approx. 3 mm; F2, 500–2000 μm; F3, 75–500 μm; F4, <75 μm. Numerical data are provided in the Supplementary Information (Tables S1 and S2). In subplot (c), horizontal bars indicate the length of the sampling period. The letter EQ indicates the time of the Great East Japan Earthquake (March-11-2011). In this subplot, the result of the preliminary study period (R1–R8) is also included. In all subplots, no lines or no marks indicate observation data do not exist.

Fig. 4 X-ray diffraction spectra of selected suspended solid samples

Symbols to peaks: V, vermiculite; M. mica; A, amphibole; K, kaolinite; Q: quartz; P, plagioclase. Subplot (a): a sample spectrum of the random orientation for major minerals analysis (sample R17, sampling period from November 26, 2012 to December 21, 2012; the size fraction F3, 75–500 μm). Subplot (b): a sample spectrum of the powder orientation for clay minerals identification for size fraction F4 (<75 μm) of the identical sampling occasion (R17). Subplot (c): spectra of the all analyzed size fractions F4 by powder orientation.

Fig. 5 Results of the chemical extraction of ^{137}Cs associated with suspended solids

Black bars: the proportion of extracted ^{137}Cs to that of the original suspended solids tested. Gray bars: ^{137}Cs concentration of the original suspended solids tested. Extraction conditions: extractant, 1 M ammonium acetate (pH 7.0); operation, 2 h at 25°C; solid solution ratio, 1 (g) vs. 10 (mL), according to Andersson and Roed (1994). The F4 size fraction of R19 and F3 of R20 were not tested because an insufficient sample amount was available.

Fig. 6 Relationship of ^{137}Cs concentration associated with suspended solids to environmental conditions.

Subplot (a), relationship to daily-normalized precipitation;; to river water discharge (d). (c), to SS mass load (c). Legend given in subplot (b) is common for subplots (a) and (b).

Fig. 7 Fluvial transport load of ^{137}Cs associated with suspended solids

Legend: F1, 2000 μm (2 mm) – approx. 3 mm; F2, 500–2000 μm; F3, 75–500 μm; F4, <75 μm. The values of the load are the daily-normalized values of the sampling occasion. For each sampling period, see Table 1.

Fig. A1 Regression of turbidity for the stream water flow rate during selected rainfall events.

The selected rainfall events are listed in Table A2.

Click here to download Figure Fig 1.pdf

Matsunaga et al.

Color on the Web, and in print.

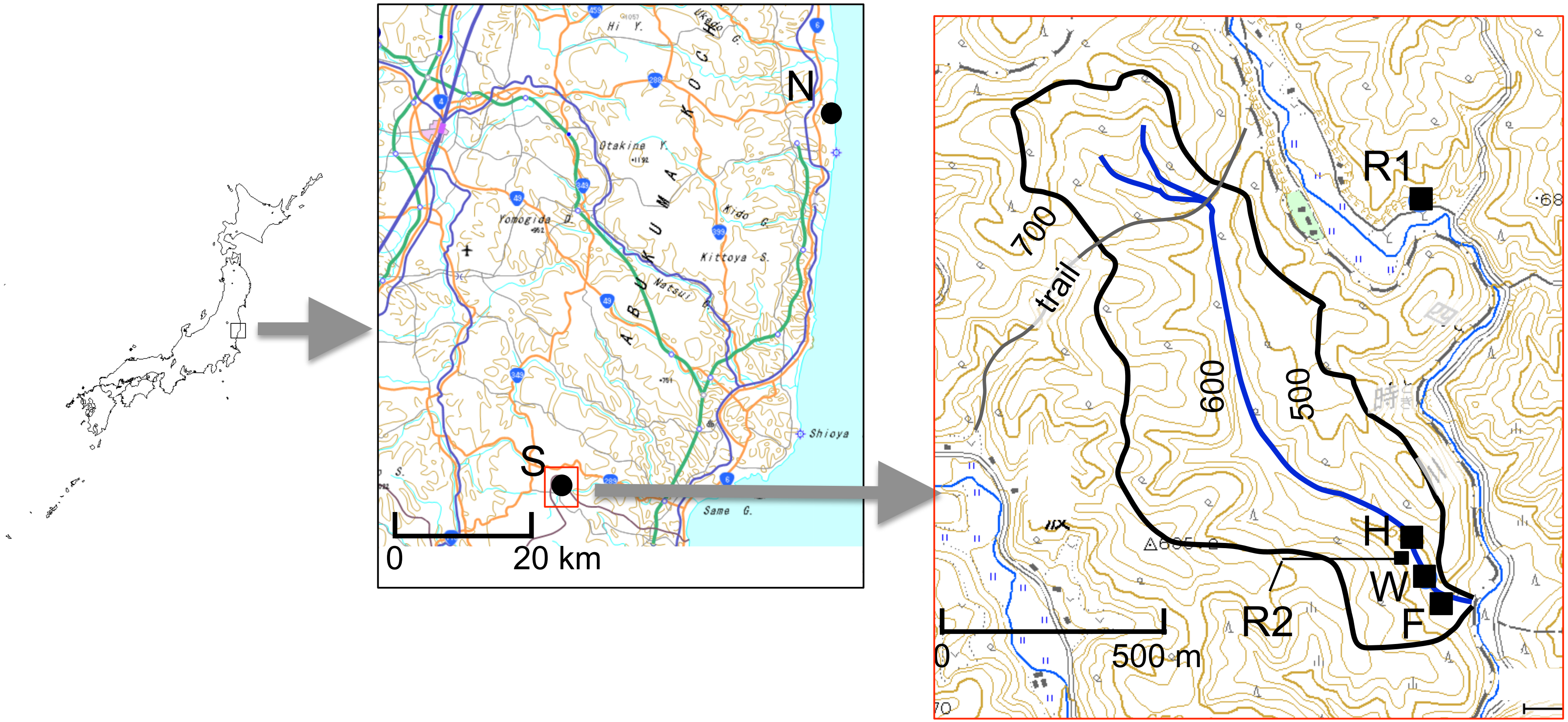

(a) (b) (c)

Fig. 1

Figure

Click here to download Figure Fig 2.pdf

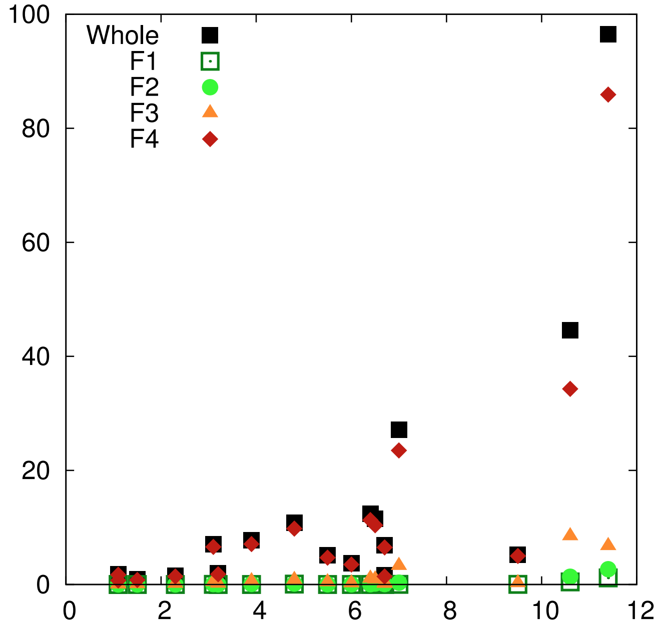

Matsunaga et al.

Color on the Web, and in print.

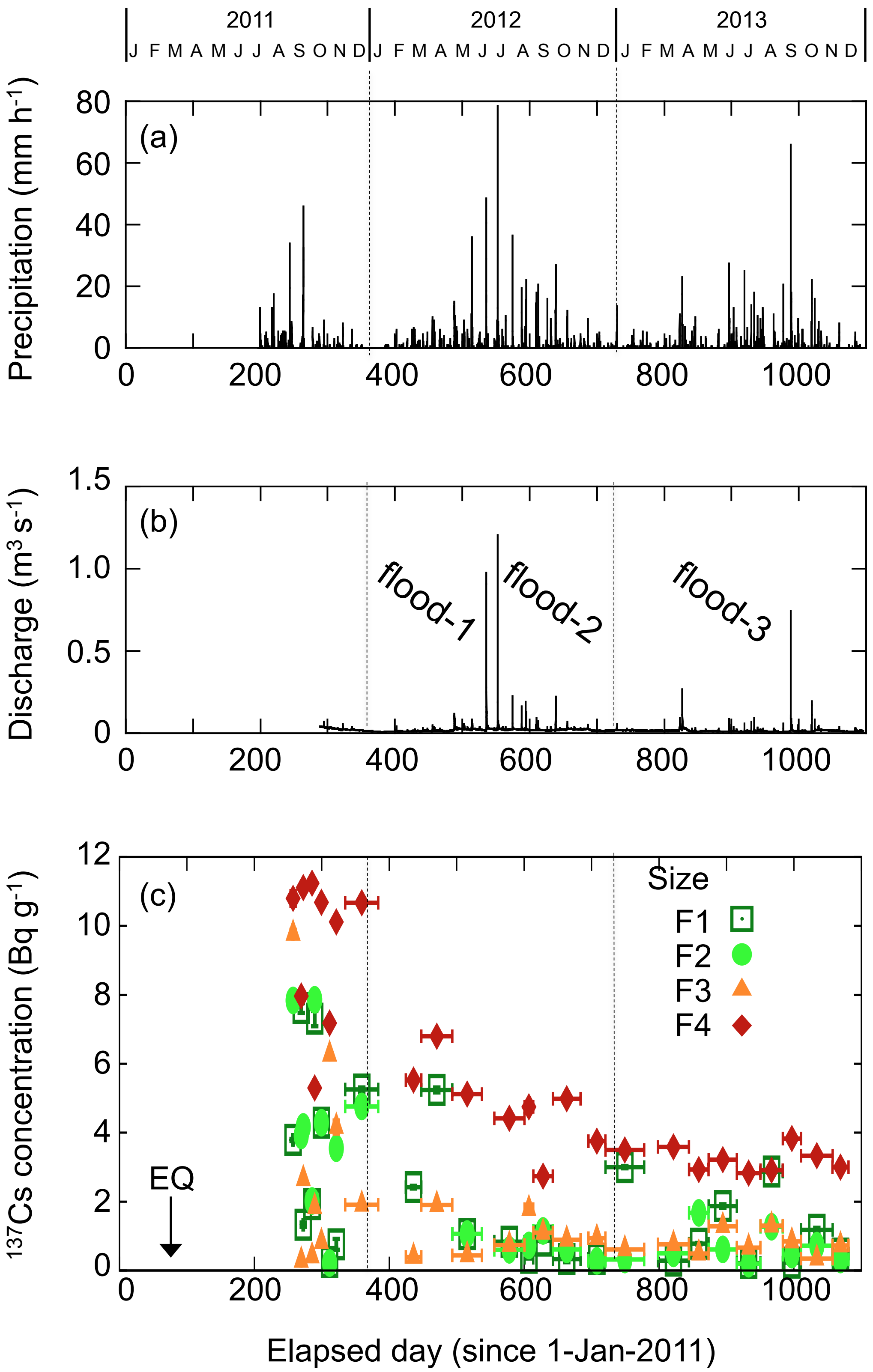

Fig. 3

Click here to download Figure Fig 4.pdf

Matsunaga et al.

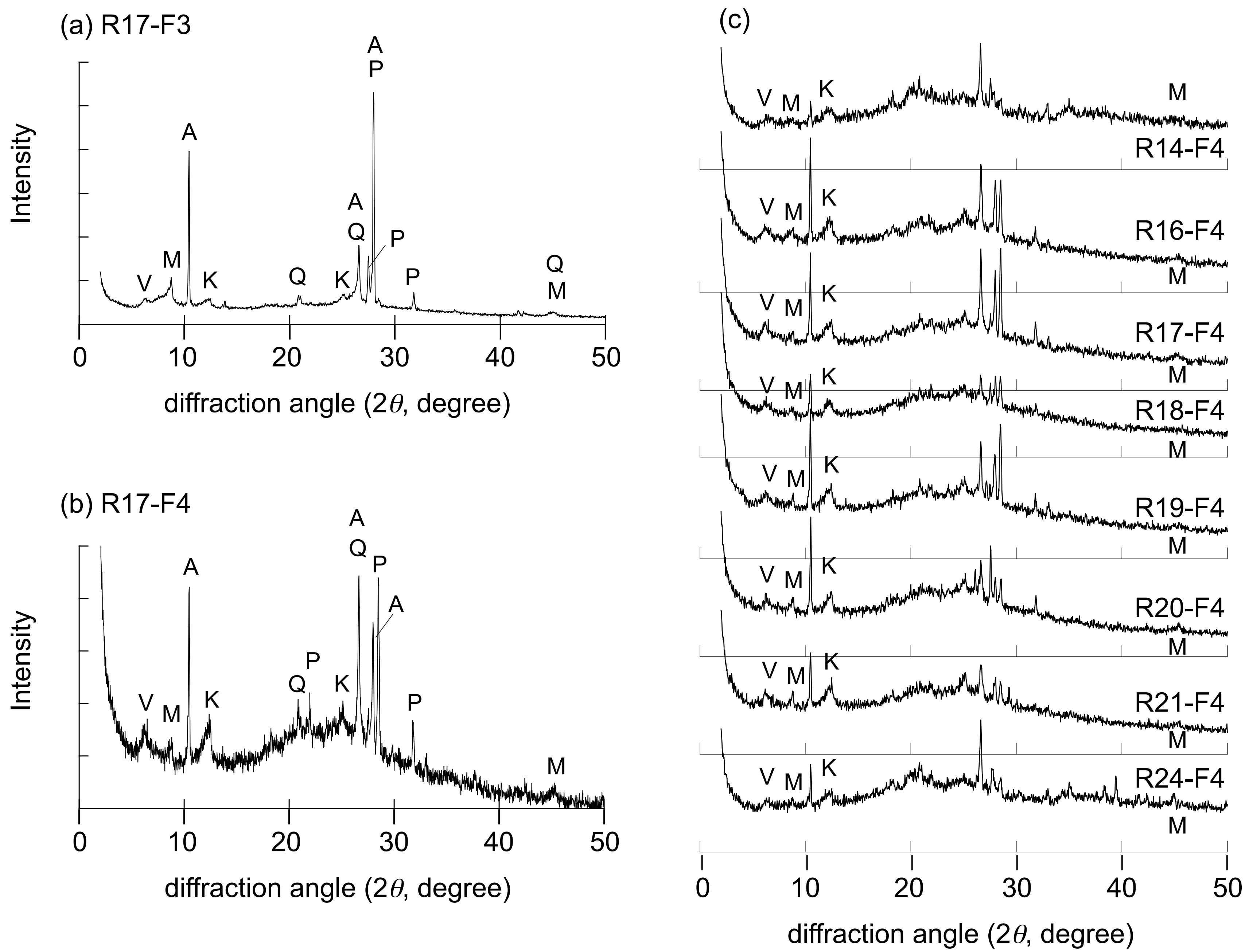

Fig. 4

Figure

Click here to download Figure Fig 5.pdf

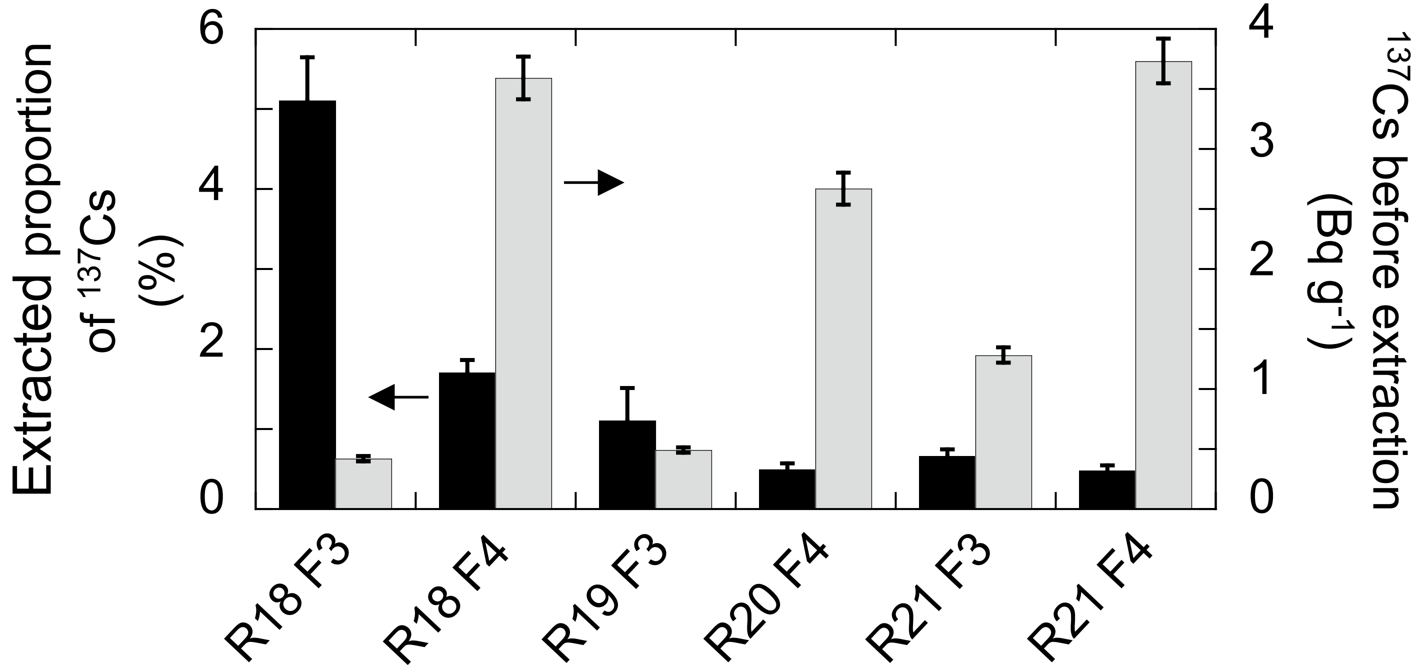

Fig. 5

Click here to download Figure Fig 6.pdf

Matsunaga et al.

Color on the Web, and in print.

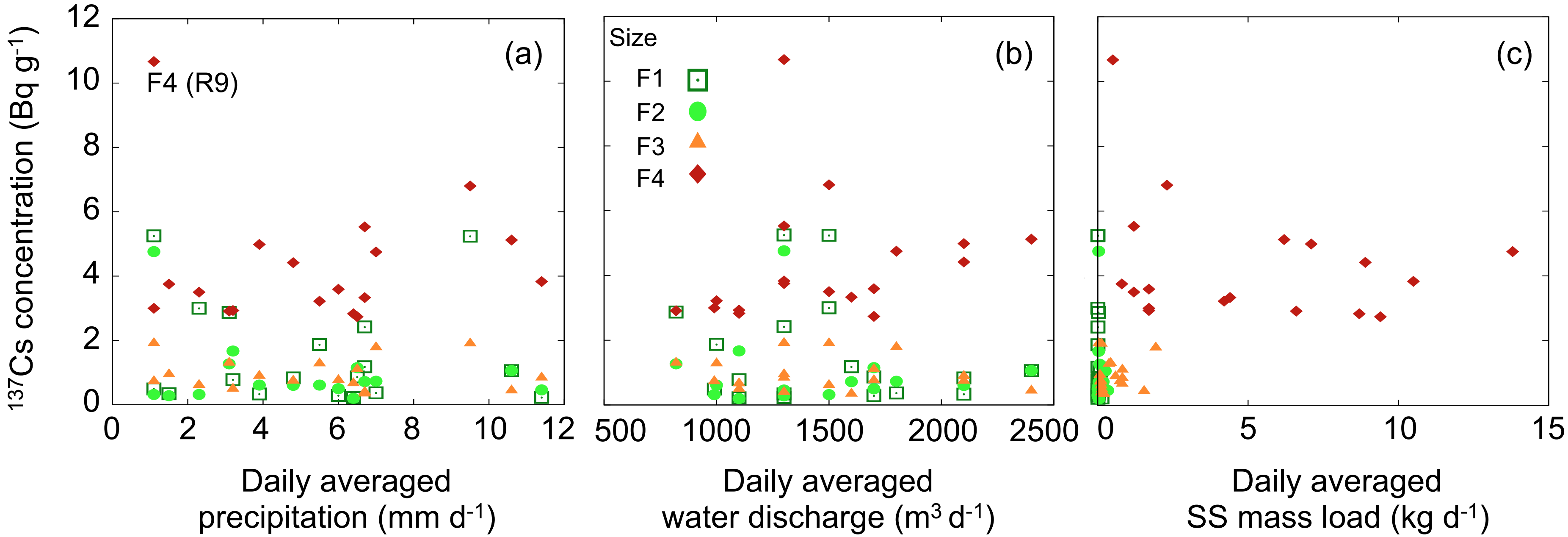

Fig. 6

Color on the Web, and in print.

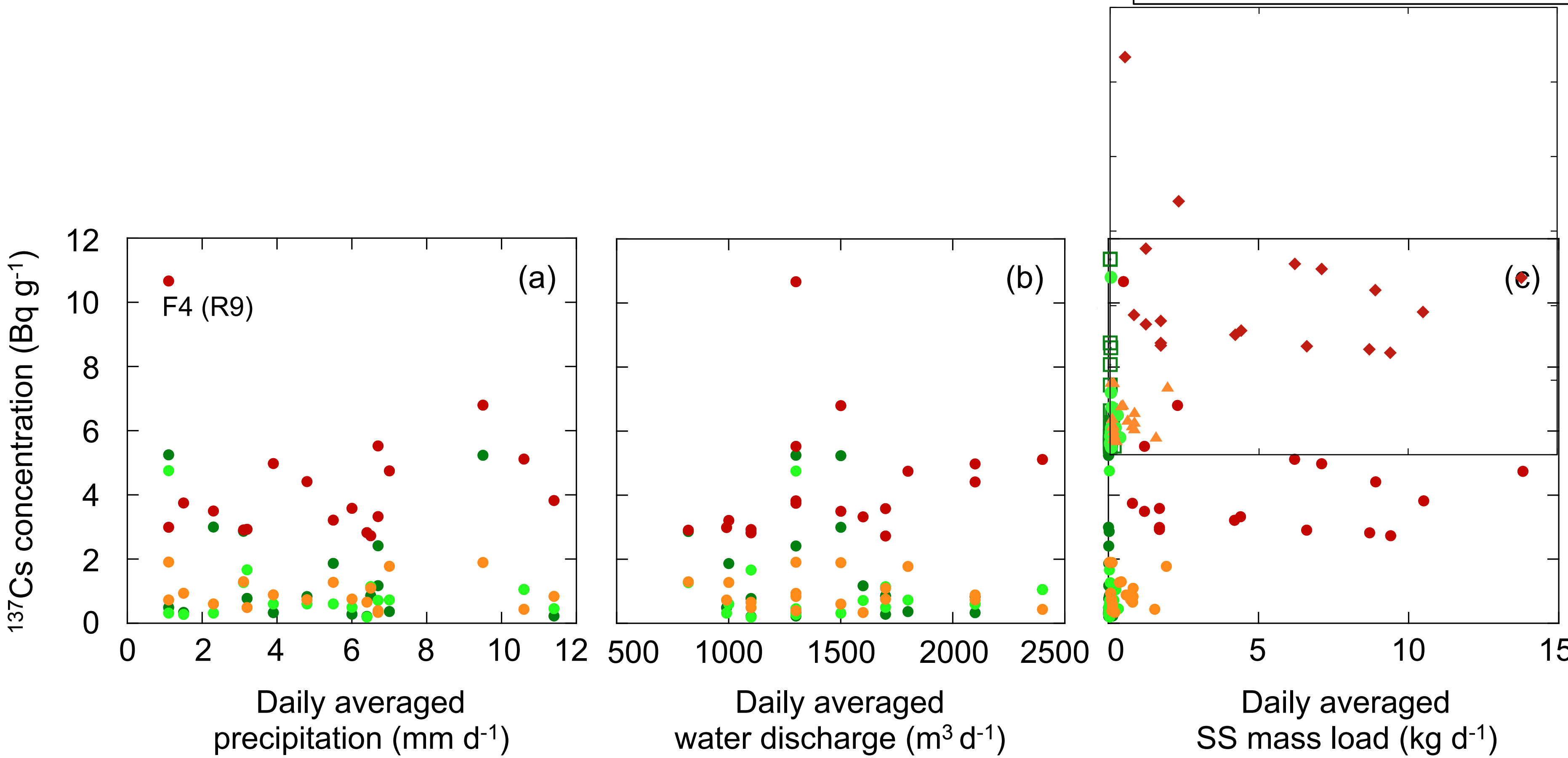

Fig. 6

Click here to download Figure Fig 7.pdf

Matsunaga et al.

Color on the Web, and in print.

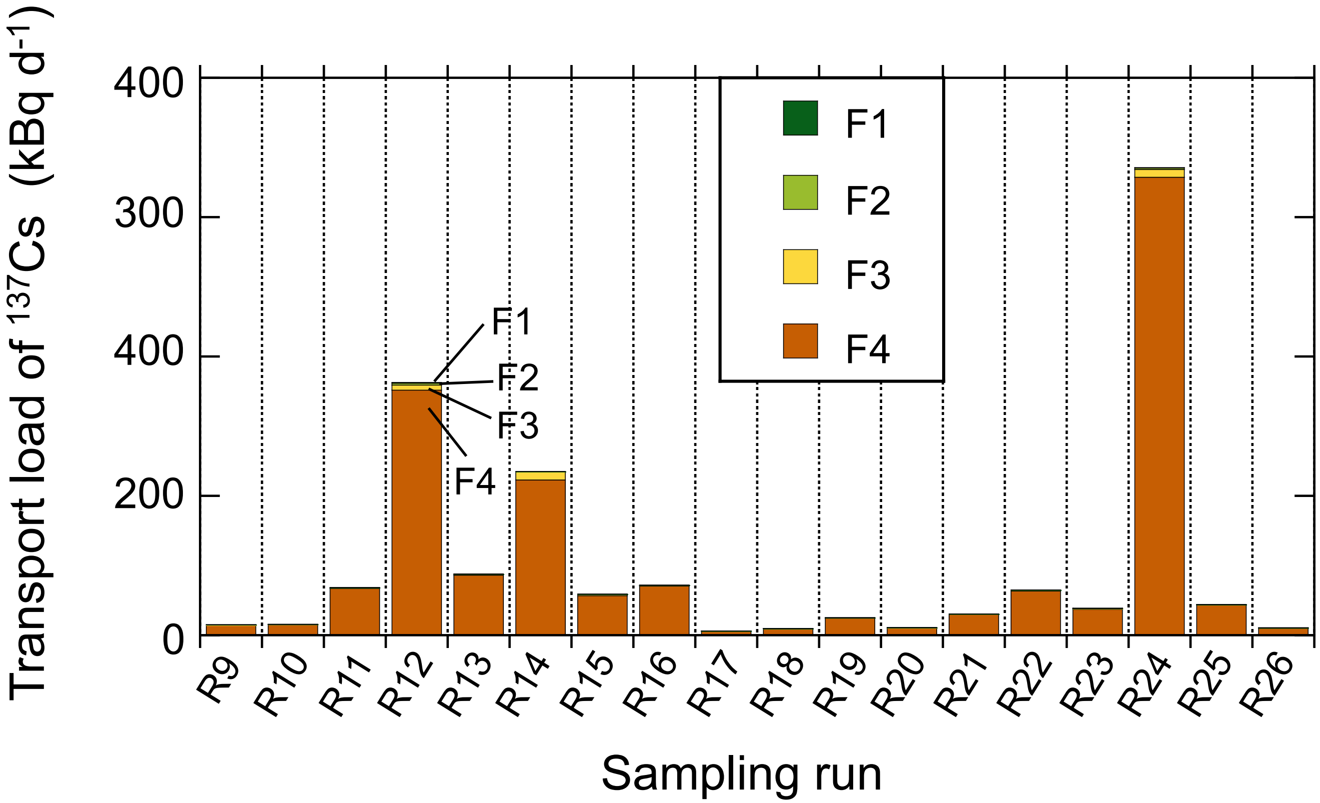

Fig. 7

Click here to download Figure Fig A1.pdf

Matsunaga et al.

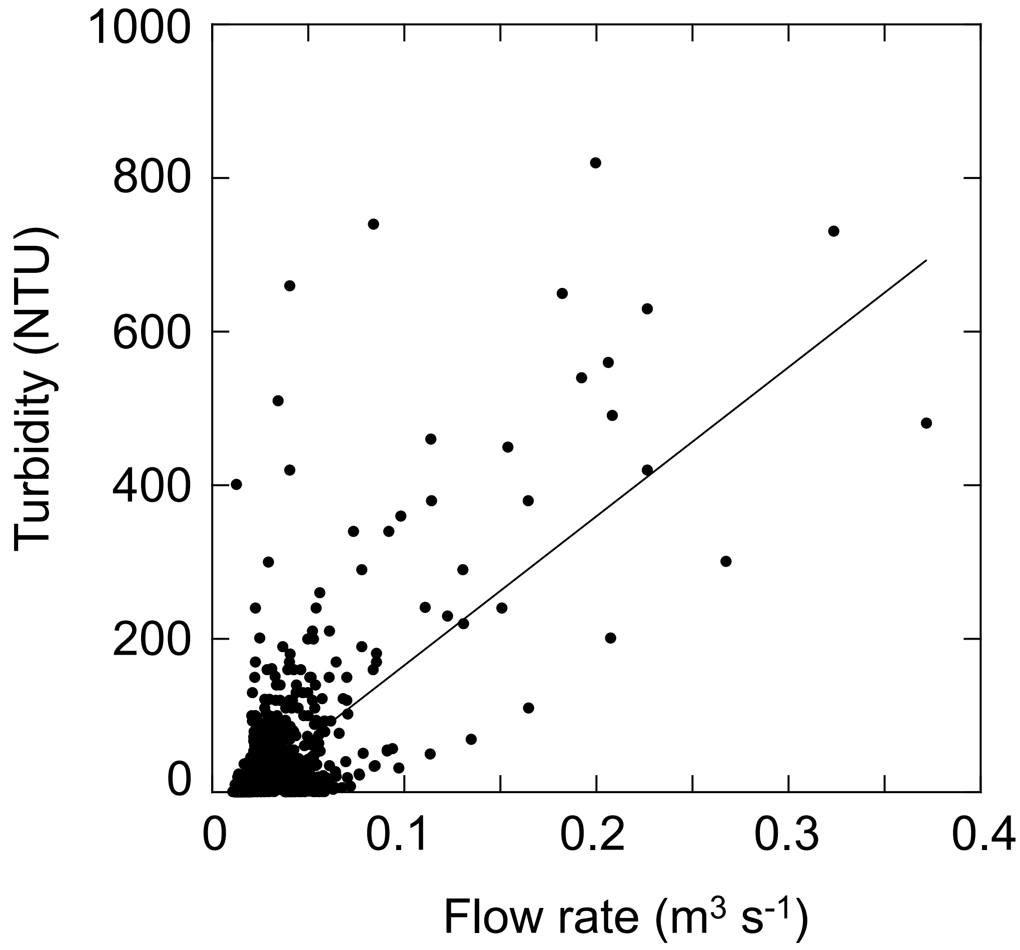

Fig. A1

Table 1 Daily averaged transport load of suspended solid and corresponding hydrologcal record

Sampling period and collection data						Hydrological record				Mass transport load of suspended solid (SS)				
Sampling			Duration (days)	Passed water (m^3)	Collected total SS (g)	Precipitation			Discharge					
						Daily average (mm $days^{-1}$)	Total in the period (mm)	Maximun intensity (mm h^{-1})	Daily average (m^3 $days^{-1}$)	Mass load (kg $days^{-1}$)	Size fraction[a] (%)			
Run #	Start	End								Total	F1	F2	F3	F4
R9	01-Dec-2011	19-Jan-2012	48.8	106.6	45.2	1.1	52.5	6.0	1.3E + 02	0.8	1.4	5.8	4.7	88.1
R10	29-Feb-2012	23-Mar-2012	23.0	67.4	69.3	6.7	154.5	6.5	1.3E + 03	1.6	0.5	9.5[b]		90.0
R11	23-Mar-2012	08-May-2012	45.8	113.9	176.8	9.5	437.0	15.0	1.5E + 03	5.2	0.2	5.0[b]		94.7
R12	08-May-2012	21-Jun-2012	44.0	127.1	437.0	10.6	466.0	48.5	2.4E + 03	44.6	1.0	3.1	19.0	76.9
R13	09-Jul-2012	23-Aug-2012	44.8	84.3	400.2	4.8	216.0	36.5	2.1E + 03	10.8	0.6	1.5	7.5	90.0
R14	23-Aug-2012	05-Sep-2012	12.8	38.8	336.8	7.0	89.5	20.5	1.8E + 03	27.1	0.1	1.2	12.1	86.7
R15	05-Sep-2012	04-Oct-2012	29.0	78.3	484.5	6.5	188.0	27.0	1.7E + 03	11.5	0.3	1.5	7.8	90.4
R16	04-Oct-2012	14-Nov-2012	41.0	131.6	499.4	3.9	161.0	12.0	2.1E + 03	7.8	0.1	1.0	7.5	91.4
R17	26-Nov-2012	21-Dec-2012	25.0	69.6	46.4	1.5	36.5	5.0	1.3E + 03	0.9	0.3	0.8	7.8	91.1
R18	21-Dec-2012	16-Feb-2013	57.4	158.3	143.7	2.3	134.0	13.5	1.5E + 03	1.5	0.3	0.8	9.1	89.9
R19	09-Mar-2013	24-Apr-2013	46.0	80.9	86.2	6.0	276.5	23.0	1.7E + 03	3.7	0.2	0.7	5.9	93.3
R20	24-Apr-2013	23-May-2013	28.8	65.7	111.0	3.2	93.0	10.0	1.1E + 03	2.0	0.3	1.5	7.4	90.7
R21	23-May-2013	04-Jul-2013	41.8	66.4	305.6	5.5	230.0	27.5	1.0E + 03	5.1	0.1	0.7	7.9	91.3
R22	04-Jul-2013	08-Aug-2013	35.0	66.3	576.0	6.4	225.5	26.0	1.1E + 03	12.4	0.1	0.4	8.5	91.0
R23	08-Aug-2013	10-Sep-2013	33.1	57.6	498.6	3.1	101.5	20.5	8.2E + 02	7.1	0.3	0.9	6.0	92.8
R24	10-Sep-2013	07-Oct-2013	26.9	58.3	529.3	11.4	307.0	66.0	1.3E + 03	96.5	1.2	2.8	6.0	89.0
R25	07-Oct-2013	22-Nov-2013	46.0	111.2	327.0	6.7	311.5	22.0	1.6E + 03	6.9	0.2	0.8	4.5	94.5
R26	22-Nov-2013	17-Dec-2013	25.0	66.3	124.7	1.1	28.5	26.5	9.9E + 02	1.8	0.1	0.5	5.2	94.2
										Mean	0.4	1.5	8.0	90.4

To keep consistency with other majority of cases, the two fractions were combined in Table 1

[a] F1 2000 μm (2 mm)—approximately 3 mm;F2 500–2000 μm; F3 75–500 μm; F4 < 75 μm

[b] In R10 and R11, different size fracnation limits were employed: F2 800–2000 μm; F3 75–800 μm, for trial

Click here to download Table Table A1.pdf

Table A1. Correction factors for the estimated SS load by a time-integral SS collection

Sampling Run number	precipitation		Correction for sampling method		Modified mass load	
	Daily avarage (mm d^{-1})	Maximum intensity (mm h^{-1})	Ratio of two integral methods	Correction factors for under-estimation	time-integral (kg d^{-1})	flow-weighted (kg d^{-1})
9	1.1	6.0	0.73	1.4	0.6	0.8
10	6.7	6.5	0.81	1.2	1.3	1.6
11	9.5	15.0	0.47	2.2	2.4	5.2
12	10.6	48.5	0.18	5.5	8.1	44.6
13	4.8	36.5	0.88	1.1	9.8	10.8
14	7.0	20.5	0.59	1.7	15.9	27.1
15	6.5	27.0	0.94	1.1	10.4	11.5
16	3.9	12.0	0.98	1.0	7.8	7.8
17	1.5	5.0	1.00	1.0	0.9	0.9
18	2.3	13.5	0.94	1.1	1.4	1.5
19	6.0	23.0	0.48	2.1	1.8	3.7
20	3.2	10.0	0.90	1.1	1.8	2.0
21	5.5	27.5	0.92	1.1	4.6	5.1
22	6.4	26.0	0.77	1.3	9.5	12.4
23	3.1	20.5	0.97	1.0	7.1	7.1
24	11.4	66.0	0.12	8.2	11.8	96.5
25	6.7	22.0	0.67	1.5	4.6	6.9
26	1.1	26.5	1.01	1.0	1.8	1.8
Average			0.74			

Table Click here to download Table Table A2.pdf

Table A2 Selected rainfall events for elucidation of a turbidity–flow rate relationship

Events number	Event period				Precipitation
	Start		End		(mm)
1	31–Mar–2012	12:00	01–Apr–2012	7:00	34.0
2	17–May–2012	17:00	18–May–2012	18:00	48.0
3	28–May–2012	13:00	28–May–2012	22:00	15.0
4	29–May–2012	13:00	01–Jun–2012	23:00	55.5
5	18–Jul–2012	16:00	19–Jul–2012	1:00	19.5
6	28–Jul–2012	15:00	29–Jul–2012	3:00	45.0
7	16–Aug–2012	14:00	16–Aug–2012	23:00	7.0
8	17–Aug–2012	1:00	19–Aug–2012	23:00	57.5
9	02–Sep–2012	9:00	03–Sep–2012	6:00	58.0
10	04–Sep–2012	16:00	05–Sep–2012	12:00	31.5
11	18–Sep–2012	14:00	19–Sep–2012	17:00	24.0
12	23–Sep–2012	7:00	23–Sep–2012	16:15	44.5
13	17–Oct–2012	15:00	18–Oct–2012	10:00	45.0
14	28–Oct–2012	21:00	29–Oct–2012	11:00	12.0
15	06–Nov–2012	6:00	07–Nov–2012	10:00	21.0
16	17–Nov–2012	16:00	18–Nov–2012	4:00	26.0
17	29–Dec–2012	22:00	31–Dec–2012	8:00	53.5
18	02–Apr–2013	21:00	04–Apr–2013	0:00	92.0
19	06–Apr–2013	17:00	07–Apr–2013	23:00	94.0
20	27–Jul–2013	17:00	31–Jul–2013	11:00	41.0
21	01–Aug–2013	1:00	01–Aug–2013	12:00	11.0
22	19–Dec–2013	7:00	22–Dec–2013	1:00	40.5

attachment to manuscript

Click here to download attachment to manuscript Fig S1.pdf

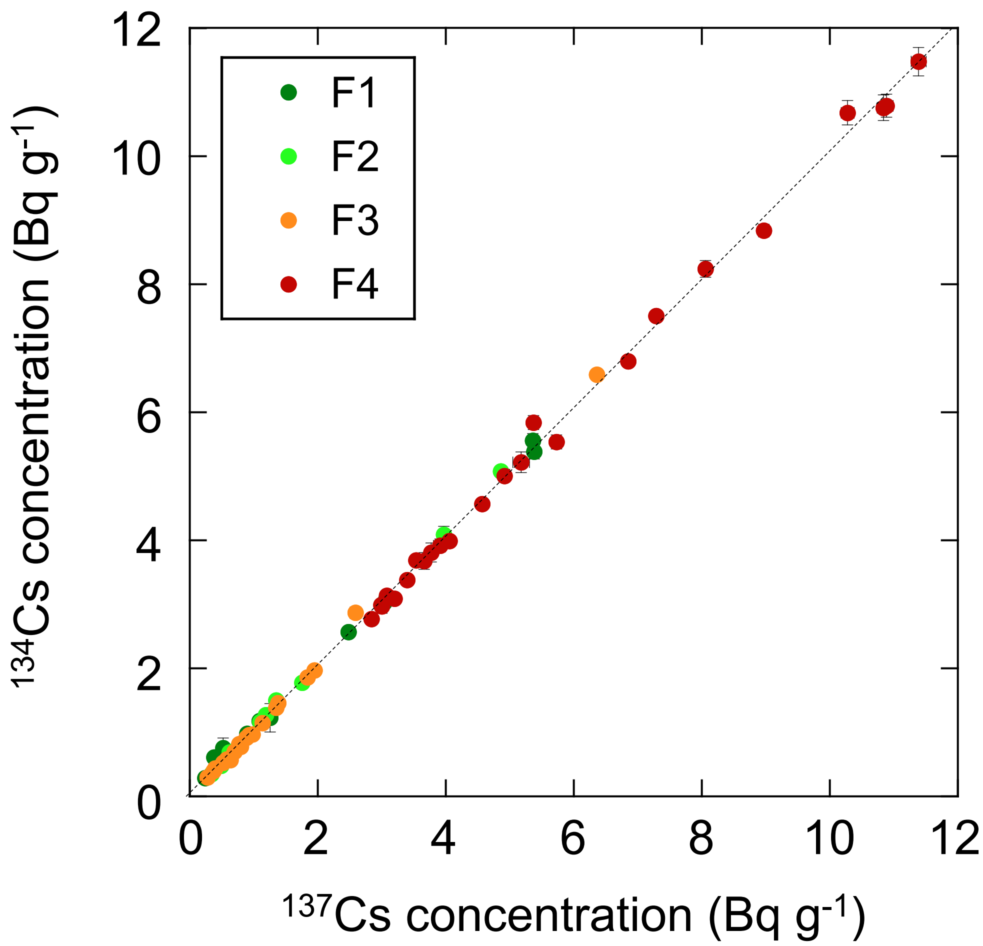

Fig. S1 Relationship between concentrations of ^{137}Cs and ^{134}Cs associated with suspended solids in the studied stream water. Radioactive concentrations are decay corrected for the day of the Great East Japan Earthquake (11-Mar-2011). Fi (i=1, 2, 3, and 4) denotes size fractions. Dashed line shows a linear regression ($y=1.00\,x + 0.04$, $R^2= 0.998$).

attachment to manuscript Click here to download attachment to manuscript Table S1.pdf

Table S1 Radioactive concentration of ^{137}Cs associated with suspended solid

			Decay corrected for the end date of sample collection				
Sampling period			Concentraion of ^{137}Cs associated with SS (Bq g^{-1})				
			Size fraction				
run number	Start	End	F1	F2	F3	F4	Average[b]
R1[a]	14-Sep-2011	26-Sep-2011	3.79 ± 0.03	7.84 ± 0.10	9.77 ± 0.12	10.8 ± 0.2	9.8 ± 0.1
R2[a]	26-Sep-2011	29-Sep-2011	7.62 ± 0.14	3.92 ± 0.07	0.28 ± 0.01	7.96 ± 0.07	3.29 ± 0.02
R3[a]	29-Sep-2011	12-Oct-2011	1.33 ± 0.06	4.17 ± 0.06	2.65 ± 0.06	11.11 ± 0.14	6.34 ± 0.07
R4[a]	12-Oct-2011	14-Oct-2011	1.93 ± 0.19	2.02 ± 0.05	0.41 ± 0.03	11.24 ± 0.12	9.9 ± 0.1
R5[a]	16-Oct-2011	19-Oct-2011	7.31 ± 0.22	7.86 ± 0.18	1.84 ± 0.04	5.30 ± 0.05	5.30 ± 0.05
R6[a]	28-Oct-2011	07-Nov-2011	4.29 ± 0.13	4.29 ± 0.13	0.83 ± 0.05	10.69 ± 0.10	9.64 ± 0.09
R7[a]	07-Nov-2011	17-Nov-2011	0.25 ± 0.03	0.22 ± 0.01	6.26 ± 0.03	7.18 ± 0.12	5.82 ± 0.01
R8[a]	17-Nov-2011	01-Dec-2011	0.76 ± 0.16	3.55 ± 0.11	4.17 ± 0.19	10.12 ± 0.10	9.39 ± 0.09
R9	01-Dec-2011	19-Jan-2012	5.25 ± 0.06	4.76 ± 0.02	1.91 ± 0.02	10.67 ± 0.10	9.84 ± 0.09
R10	29-Feb-2012	23-Mar-2012	2.42 ± 0.04	0.40 ± 0.01		5.53 ± 0.06	5.12 ± 0.05
R11	23-Mar-2012	08-May-2012	5.24 ± 0.07	1.90 ± 0.02		6.80 ± 0.03	6.44 ± 0.03
R12	08-May-2012	21-Jun-2012	1.06 ± 0.03	1.06 ± 0.01	0.44 ± 0.01	5.12 ±0.04	4.07 ± 0.03
R13	09-Jul-2012	23-Aug-2012	0.84 ± 0.02	0.60 ± 0.02	0.74 ± 0.02	4.42 ± 0.03	4.06 ± 0.03
R14	23-Aug-2012	05-Sep-2012	0.37 ± 0.02	0.73 ± 0.01	1.78 ± 0.01	4.75 ± 0.05	4.34 ± 0.05
R15	05-Sep-2012	04-Oct-2012	0.87 ± 0.03	1.15 ± 0.02	1.10 ± 0.02	2.74 ± 0.04	2.58 ± 0.03
R16	04-Oct-2012	14-Nov-2012	0.34 ± 0.09	0.61 ± 0.02	0.89 ± 0.01	4.98 ± 0.12	4.6 ± 0.1
R17	26-Nov-2012	21-Dec-2012	0.34 ± 0.04	0.28 ± 0.02	0.94 ± 0.02	3.75 ± 0.10	3.49 ± 0.09
R18	21-Dec-2012	16-Feb-2013	3.00 ± 0.03	0.32 ± 0.02	0.61 ± 0.07	3.50 ± 0.07	3.21 ± 0.06
R19	09-Mar-2013	24-Apr-2013	0.29 ± 0.06	0.50 ± 0.02	0.76 ± 0.02	3.59 ± 0.17	3.40 ± 0.07
R20	24-Apr-2013	23-May-2013	0.78 ± 0.02	1.67 ± 0.02	0.49 ± 0.01	2.93 ± 0.03	2.72 ± 0.03
R21	23-May-2013	04-Jul-2013	1.87 ± 0.05	0.61 ± 0.02	1.28 ± 0.02	3.22 ± 0.04	3.05 ± 0.04
R22	04-Jul-2013	08-Aug-2013	0.22 ± 0.07	0.20 ± 0.01	0.66 ± 0.01	2.83 ± 0.03	2.63 ± 0.03
R23	08-Aug-2013	10-Sep-2013	2.87 ± 0.05	1.27 ± 0.02	1.30 ± 0.04	2.83 ± 0.03	2.73 ± 0.03
R24	10-Sep-2013	07-Oct-2013	0.23 ± 0.01	0.46 ± 0.01	0.84 ± 0.01	3.83 ± 0.03	3.48 ± 0.02
R25	07-Oct-2013	22-Nov-2013	1.18 ± 0.06	0.72 ± 0.02	0.35 ± 0.02	3.33 ± 0.03	3.17 ± 0.03
R26	22-Nov-2013	17-Dec-2013	0.49 ± 0.06	0.32 ± 0.02	0.73 ± 0.01	3.00 ± 0.02	2.86 ± 0.02

[a] Preliminary sampling periods with a small scale filtration system. Sample collection stopped in several days due to clogging of the filters. Sampling duration was not identified.

[b] Averaged concentration over different size fractions weighed by mass contribution of each fraction (see Table 1).
Starting days of collection of R1-R8 are as follows:

Table S2 Radioactive concentration of ^{134}Cs associated with suspended solid

			Decay corrected for the end date of sample collection			
	Sampling period		Concentraion of ^{134}Cs associated with SS (Bq g^{-1})			
			Size fraction			
run number	Start	End	F1	F2	F3	F4
R1[a]	14-Sep-2011		–	–	–	–
R2[a]	26-Sep-2011			3.4 ± 0.1	0.25 ± 0.01	6.8 ± 0.1
R3[a]	29-Sep-2011		–	–	–	–
R4[a]	12-Oct-2011		–	–	–	9.4 ± 0.2
R5[a]	16-Oct-2011		–	–	–	4.8 ± 0.1
R6[a]	28-Oct-2011		–	–	–	8.7 ± 0.2
R7[a]	07-Nov-2011		–	–	5.28 ± 0.04	6.02 ± 0.03
R8[a]	17-Nov-2011		–	–	–	8.5 ± 0.2
R9	01-Dec-2011	19-Jan-2012	4.17 ± 0.08	3.81 ± 0.03	1.48 ± 0.04	8.1 ± 0.1
R10	29-Feb-2012	23-Mar-2012	1.82 ± 0.05	0.30 ± 0.01		3.92 ± 0.08
R11	23-Mar-2012	08-May-2012	3.65 ± 0.08	3.91 ± 0.05	1.94 ± 0.06	5.99 ± 0.07
R12	08-May-2012	21-Jun-2012	0.77 ± 0.04	0.76 ± 0.02	0.38 ± 0.01	4.42 ± 0.04
R13	09-Jul-2012	23-Aug-2012	–	0.42 ± 0.02	0.50 ± 0.02	2.81 ± 0.03
R14	23-Aug-2012	05-Sep-2012	0.37 ± 0.02	0.47 ± 0.01	1.13 ± 0.01	3.04 ± 0.06
R15	05-Sep-2012	04-Oct-2012	0.58 ± 0.04	0.75 ± 0.02	0.68 ± 0.02	1.64 ± 0.04
R16	04-Oct-2012	14-Nov-2012	–	–	0.55 ± 0.01	2.97 ± 0.09
R17	26-Nov-2012	21-Dec-2012	–	–	0.54 ± 0.01	2.16 ± 0.06
R18	21-Dec-2012	16-Feb-2013	–	–	0.30 ± 0.02	1.92 ± 0.07
R19	09-Mar-2013	24-Apr-2013	–	–	0.38 ± 0.02	1.87 ± 0.08
R20	24-Apr-2013	23-May-2013	–	0.85 ± 0.02	0.25 ± 0.01	1.50 ± 0.03
R21	23-May-2013	04-Jul-2013	–	0.32 ± 0.02	0.64 ± 0.02	1.56 ± 0.03
R22	04-Jul-2013	08-Aug-2013	–	–	0.31 ± 0.01	1.33 ± 0.03
R23	08-Aug-2013	10-Sep-2013	1.31 ± 0.04	0.65 ± 0.02	0.63 ± 0.04	1.28 ± 0.05
R24	10-Sep-2013	07-Oct-2013	0.12 ± 0.01	0.20 ± 0.01	0.39 ± 0.01	1.68 ± 0.02
R25	07-Oct-2013	22-Nov-2013	0.50 ± 0.09	0.32 ± 0.01	0.16 ± 0.02	1.49 ± 0.03
R26	22-Nov-2013	17-Dec-2013	0.30 ± 0.06	0.14 ± 0.02	0.31± 0.01	1.22 ± 0.02

[a] Preliminary sampling periods with a small scale filtration system. Sample collection stopped in several days after the start day due to clogging of the filters. End of sampling date was not identified.

attachment to manuscript Click here to download attachment to manuscript Table S3.pdf

Table S3 Decay correction factors for the stardard day of 11-Mar-2011 (the day the Great East Japan Earthquake)

Sampling		Day numbers since 11-Mar-2011	Decay cooroection for 11-Mar-2011	
			Decay correction factors	
run number	End date		^{137}Cs	^{134}Cs
R1	26-Sep-2011	187	0.988	0.842
R2	29-Sep-2011	199	0.988	0.833
R3	12-Oct-2011	202	0.987	0.831
R4	14-Oct-2011	215	0.987	0.821
R5	19-Oct-2011	219	0.986	0.818
R6	07-Nov-2011	231	0.986	0.809
R7	17-Nov-2011	241	0.985	0.801
R8	01-Dec-2011	251	0.984	0.794
R9	19-Jan-2012	315	0.980	0.749
R10	23-Mar-2012	378	0.976	0.707
R11	08-May-2012	424	0.974	0.677
R12	21-Jun-2012	468	0.971	0.650
R13	23-Aug-2012	531	0.967	0.614
R14	05-Sep-2012	544	0.966	0.607
R15	04-Oct-2012	573	0.964	0.591
R16	14-Nov-2012	614	0.962	0.569
R17	21-Dec-2012	651	0.960	0.550
R18	16-Feb-2013	708	0.956	0.522
R19	24-Apr-2013	775	0.952	0.491
R20	23-May-2013	804	0.950	0.478
R21	04-Jul-2013	846	0.948	0.460
R22	08-Aug-2013	881	0.946	0.445
R23	10-Sep-2013	914	0.944	0.432
R24	07-Oct-2013	941	0.942	0.421
R25	22-Nov-2013	987	0.940	0.404
R26	17-Dec-2013	1012	0.938	0.395
	Saito et al., 2011 14-Jun-2011[a]	95	0.994	0.916

[a] The standard day for decay correction to deduce a radioactivity ratio of ^{134}Cs to ^{137}Cs. The ratio is given 0.91 as of the date 14-Jun-2011 in the literature (Saito et al., 2015). This ratio is equvalent to 0.99 as of the date 11-Mar-2011.

attachment to manuscript Click here to download attachment to manuscript Table S4.pdf

Table S4 Result of collection efficiency evaluation

Decay corrected for the end date of sample collection										
	Sampling period		Collected radioacitivity of Cs-137 with SS by the main collection system (A) (Bq)					Collected radioacitivity of Cs-137 with SS by the backup filters* (B) (Bq)	Uncollected proportion** B/(A+B) (%)
run			Size fraction						
number	Start	End	F1	F2	F3	F4	Sum		
R24	10-Sep-2013	07-Oct-2013	1.46	6.79	31.1	1370	1410	14.4	1.0
R25	07-Oct-2013	22-Nov-2013	0.70	1.93	5.11	1182	1190	7.7	0.6
R26	22-Nov-2013	17-Dec-2013	0.06	0.21	4.73	352	357	5.8	1.6

[a] backup filters : a set of short cartridge filters (250 mm length) after the main collection system.

[b] the sum of A and B was taken as 100%.

attachment to manuscript Click here to download attachment to manuscript Table S5.pdf

Table S5 Fluvial transport load of ^{137}Cs associated with suspended solid

Sampling period			Transport load of ^{137}Cs (Bq d^{-1})				
run number	Start	End	Size fraction				
			F1	F2	F3	F4	whole SS
R9	01-Dec-2011	19-Jan-2012	5.9E+01	2.1E+02	7.0E+01	5.2E+03	7.3E+03
R10	29-Feb-2012	23-Mar-2012	1.9E+01	5.5E+01		6.6E+03	7.9E+03
R11	23-Mar-2012	08-May-2012	6.1E+01	5.0E+02		1.5E+04	3.4E+04
R12	08-May-2012	21-Jun-2012	4.9E+02	1.4E+03	3.7E+03	3.2E+04	1.8E+05
R13	09-Jul-2012	23-Aug-2012	5.0E+01	9.8E+01	6.0E+02	3.9E+04	4.3E+04
R14	23-Aug-2012	05-Sep-2012	1.0E+01	2.3E+02	5.8E+03	6.6E+04	1.1E+05
R15	05-Sep-2012	04-Oct-2012	3.0E+01	2.0E+02	9.9E+02	2.6E+04	2.8E+04
R16	04-Oct-2012	14-Nov-2012	2.1E+00	4.9E+01	5.2E+02	3.6E+04	3.6E+04
R17	26-Nov-2012	21-Dec-2012	7.8E-01	2.0E+00	6.4E+01	3.0E+03	3.0E+03
R18	21-Dec-2012	16-Feb-2013	1.5E+01	3.7E+00	8.4E+01	4.3E+03	4.8E+03
R19	09-Mar-2013	24-Apr-2013	1.9E+00	1.2E+01	1.7E+02	6.0E+03	1.3E+04
R20	24-Apr-2013	23-May-2013	5.2E+00	5.1E+01	7.3E+01	4.9E+03	5.4E+03
R21	23-May-2013	04-Jul-2013	1.2E+01	2.1E+01	5.2E+02	1.4E+04	1.5E+04
R22	04-Jul-2013	08-Aug-2013	1.6E+00	1.0E+01	7.0E+02	2.5E+04	3.2E+04
R23	08-Aug-2013	10-Sep-2013	6.9E+01	7.9E+01	5.6E+02	1.9E+04	1.9E+04
R24	10-Sep-2013	07-Oct-2013	2.7E+02	1.2E+03	5.7E+03	4.0E+04	3.3E+05
R25	07-Oct-2013	22-Nov-2013	1.5E+01	4.1E+01	1.1E+02	1.4E+04	2.2E+04
R26	22-Nov-2013	17-Dec-2013	8.8E-01	3.1E+00	7.0E+01	5.2E+03	5.2E+03